Prompt gamma-ray emission of GRB 170817A associated with GW 170817: a consistent picture

Houri Ziaeepour

Monthly Notices
of the
ROYAL ASTRONOMICAL SOCIETY

MNRAS **478,** 3233–3252 (2018)
Advance Access publication 2018 May 14

doi:10.1093/mnras/sty1246

Prompt gamma-ray emission of GRB 170817A associated with GW 170817: a consistent picture

Houri Ziaeepour[1,2]★

[1]*Institut UTINAM, CNRS UMR 6213, Observatoire de Besançon, Université de Franche Compté, 41 bis ave. de l'Observatoire, BP 1615, F-25010 Besançon, France*
[2]*Mullard Space Science Laboratory, Holmbury St Mary, Dorking, Surrey RH5 6NT, UK*

Accepted 2018 May 10. Received 2018 May 10; in original form 2018 January 23

ABSTRACT

The short GRB 170817A associated with the first detection of gravitation waves from a binary neutron star (BNS) merger was in many ways unusual. Possible explanations are emission from a cocoon or cocoon break out, off-axis view of a structured or uniform jet, and on-axis ultra-relativistic jet with reduced density and Lorentz factor. Here, we use a phenomenological model of shock evolution and synchrotron/self-Compton emission to simulate the prompt emission of GRB 170817A and to test above proposals. We find that synchrotron emission from a mildly relativistic cocoon with a Lorentz factor of 2–3, as considered in the literature, generates a too soft, too long, and too bright prompt emission. Off-axis view of a structured jet with a Lorentz factor of about 10 can reproduce observations, but needs a very efficient transfer of kinetic energy to electrons in internal shocks, which is disfavoured by particle in cell simulations. We also comment on cocoon breakout as a mechanism for generation of the prompt gamma-ray. A relativistic jet with a Lorentz factor of about 100 and a density lower than typical short GRBs seems to be the most plausible model and we conclude that GRB 170817A was intrinsically faint. Based on this result and findings of relativistic magnetohydrodynamics simulations of BNS merger in the literature we discuss physical and astronomical conditions, which may lead to such faint short GRBs. We identify small mass difference of progenitor neutron stars, their old age and reduced magnetic field, and anti-alignment of spin–orbit angular momentum induced by gravitational disturbances during the lifetime of the BNS as causes for the faintness of GRB 170817A. We predict that BNS mergers at lower redshifts generate on average fainter GRBs.

Key words: gamma-ray burst – gravitational wave – binary neutron star – merger – relativistic shock.

1 INTRODUCTION

The discovery of the gravitational wave (GW) event GW 170817 (LIGO Scientific Collaboration & Virgo Scientific Collaboration 2017a) and accompanying electromagnetic transient GRB 170817A (Goldstein et al. 2017; LIGO Scientific Collaboration 2017a,b; Savchenko et al. 2017), and its afterglow in X-ray (Evans et al. 2017; Haggard et al. 2017; Troja et al. 2017) and other energy bands (Alexander et al. 2017; Arcav et al. 2017; Buckley et al. 2017; Chornock et al. 2017; Coulter et al. 2017; Guidorzi et al. 2017; Hallinan et al. 2017; Kasen et al. 2017; Kasliwal et al. 2017a; Pian et al. 2017; Soares-Santos et al. 2017; Valenti et al. 2017; Pozanenko et al. 2018) are revolutionizing astronomy and fundamental physics. Association of GW 170817 to merger of a binary neutron star (BNS), based on the masses of the progenitors and the length of GW event, is the first direct evidence for formation of short GRBs by collision and merging of ultra-compact astronomical objects. Although observation of supernova-like behaviour of late time afterglow of long GRBs has confirmed the hypothesis of their formation during core collapse of massive stars, a direct evidence for the origin of short GRBs had to wait the historic detection of GW/GRB 170817A.

Despite excitements about its observation, GRB 170817A is very far from being a typical representative of hundreds of short GRB events detected during the past three decades or so by high energy space observatories such as BATSE (Fishman et al. 1989), Neil Gehrels *Swift* Observatory (Gehrels et al. 2004), *Fermi* (Dingus 1995), Integral (Winkler et al. 2003), Konus Wind (Aptekar et al. 1995), etc. It is much softer than most short GRBs, a few orders of magnitude fainter than short bursts with known redshift, and falls on

★ Email: houriziaeepour@gmail.com

the boundary of short–long GRB separation. The unusual characteristics of GRB 170817A are evidently noticed and widely discussed in the articles published immediately after the announcement of GW/GRB 170817 detection.

The simplest explanation is an off-axis view (Lamb & Kobayashi 2017) of a uniform (top hat) or structured ultra-relativistic jet similar to those of other short GRBs (Pian et al. 2017). Alternatively, the burst might have been formed by a mildly relativistic magnetized cocoon (Gottlieb et al. 2017; Kasliwal et al. 2017a) at its breakout (Nakar & Sari 2012). However, it seems an extra-ordinary coincidence if we have detected an off-axis GRB or one generated by the cocoon breakout in the first detection of GWs from a BNS merger. Although (Lazzati et al. 2017a,b; Kathirgamaraju, Barniol Duran & Giannios 2018) argue that due to the small opening angle of relativistic jets, electromagnetic counterparts of GW events from binary mergers must be dominated by relatively soft emission of a jet viewed off-axis or a cocoon or sheath surrounding the jet, X-ray light curves for simulated afterglows with non-zero viewing angle (Cuesta-Martínez, Aloy & Mimica 2015a; Cuesta-Martínez et al. 2015b;Lazzati et al. 2017a) deviate significantly from *Swift*-XRT observations of more than 100 short GRBs followed up by this instrument so far, including kilonova/GRB 130603B (Kennea et al. 2013) (see also Sections 3 and 7 for further discussion).

Evidence for (semi-)thermal emission from a cocoon (Nakar & Sari 2012) is also very rare and mostly in low energies. Therefore, either most short GRBs belong to a completely different population, or the dynamics of their progenitors is such that the probability of a close to on-axis view is large. In conclusion, although with a statistical sample of one event it is not possible to rule out a rare coincidence of GW with off-axis or cocoon emission, we should consider other possibilities.

In this work we first briefly review observed properties of GRB 170817A in Section 2 and compare them with those of other short GRBs. This opens our discussion and arguments in Section 3 about the small probability that faint soft short GRBs such as GRB 170817A be off-axis view of an otherwise normal GRB. We raise other possibilities as reasons behind faintness and softness of some short GRBs, including GRB 170817A, which have their root in the physics of formation and acceleration of jets, and production of GRB emission. In Section 4 we use a phenomenological model for formation and evolution of GRB emission by internal shocks (Ziaeepour 2009; Ziaeepour & Gardner 2011) to simulate the prompt emission of GRB 170817A and compare simulation parameters with those of GRB 130603B – the only other short GRB with evidence of an accompanying kilonova (Berger, Fong & Chornock 2013; Tanvir et al. 2013; Metzger 2017). The aim of this exercise is to have a quantitative estimation of physical properties of GRB producing processes and their progenitor stars, notably jet density, Lorentz factor, and Poynting energy, which can be compared with findings of BNS merger simulations. Results of our simulations are discussed and interpreted in Section 5. In Section 6 we use conclusions of 3D General Relativistic Magneto-Hydro-Dynamics (GRMHD) simulations from literature to investigated which configuration and properties of progenitors may lead to a thin jet with a relatively low Lorentz factor, as estimated for GRB 170817A. Implications of our findings are discussed in Section 7. We provide an overall qualitative picture of GW/GRB 170817 event and its difference with intrinsically brighter GRBs. Outlines and prospectives are presented in Section 8.

2 GRB AND OTHER ELECTROMAGNETIC EMISSIONS

GRB 170817A was detected by the GBM detector of the *Fermi* satellite (Goldstein et al. 2017) about 1.7 s after the end of GW event GW 170817. It lasted for about 2 s, had an integrated fluence in 10 keV to 1 MeV band of $(2.8 \pm 0.2) \times 10^{-7}$ erg cm^{-2} (Goldstein et al. 2017) [$(1.4 \pm 0.4 \pm 0.6) \times 10^{-7}$ erg cm^{-2} in Integral-IBIS 75 keV to 2 MeV band (Savchenko et al. 2017)], a photon count rate of 3.7 ± 0.9 photon s^{-1} cm^{-2} for 64 ms binning, and its peak energy was $E_{\rm peak} = 229 \pm 78$ keV (Goldstein et al. 2017). In comparison with other short GRBs these characteristics correspond to properties of a mildly faint short GRB, see Fig. 1(a,b). The follow up of this event by a plethora of ground- and space-based telescopes (LIGO Scientific Collaboration 2017a,b) allowed to find the optical/IR/radio counterparts AT 2017 gfo, its host galaxy NGC 4993, and thereby its redshift $z = 0.0095$ and its distance of $\sim$40 Mpc,[1] making GRB 170817A the closest GRB with known distance so far, see e.g. Berger (2014) for a review of properties of short GRBs and their hosts. Using the distance to the host galaxy, GRB 170817A had an isotropic luminosity $E_{\rm iso} \sim 5 \times 10^{46}$ erg in 10 keV to 1 MeV band, which makes it the most intrinsically faint short burst with known redshift, see Fig. 1(c,d). Moreover, the peak energy of the burst is close to lowest peak energy of short bursts observed by *Fermi*-GBM (see fig. 31 in Gruber et al. 2014).

Unfortunately at the time of prompt emission GRB 170817A was not in the field of view of *Swift*-BAT and no early follow-up observation is available, except for an upper limit of $>4\sigma$ on any excess from background in the time interval ($T + 2.944$, $T+ 100$) s, where T is the prompt gamma-ray trigger time, in 10 keV to 10 MeV band – assuming $E_{\rm peak}= 128$ keV and a CPL spectrum for this time interval – from Konus-Wind satellite (Svinkin et al. 2017). Indeed, even in the time interval of detection by *Fermi*-GBM and Integral-IBIS, the burst was too faint for Konus-Wind and only an upper limit is reported (Svinkin et al. 2017).

2.1 X-ray counterpart

The earliest observation of GW/GRB 170817A in X-ray was at about $T + 0.6$ d $=T+ 51840$ s (Evans et al. 2017). None the less, from preliminary observations by the *Swift*-XRT in the sky area calculated from GW observations by the Advanced LIGO–Virgo, a flux limit of $\sim 10^{-12}$erg s^{-1} cm^{-2} in 0.3–10 keV band can be put on the X-ray afterglow of GRB 170817A around $T + 0.2$ d. There is also an upper flux limit of 3.5×10^{-15}erg s^{-1} cm^{-2} at $\sim T + 2$ d for any X-ray afterglow (Margutti et al. 2017).

Although the X-ray afterglow of some short GRBs have been brighter than these limits, others, e.g. GRB 070724A (Ziaeepour et al. 2007; Berger et al. 2009; Kocevski et al. 2010), GRB 111020A (Sakamoto et al. 2011), GRB 130912A (D'Elia et al. 2013; Zhu et al. 2015), and GRB 160821B (Siegel et al. 2016; Kasliwal et al. 2017b) had smaller fluxes at $\sim$0.3 d after trigger. GRB 111020A is an interesting case because its host galaxy is most probably at redshift 0.02 (Tunnicliffe et al. 2014). Therefore, its progenitor stars might have had properties similar to those of the progenitors of GRB 170817A. It had a total gamma-ray fluence about 50 per cent less than GRB 170817A, but an average flux about three times larger than the latter. It was observed by the *Swift*-XRT from $\sim T+ 100$ s up to $\sim T + 3 \times 10^5$ s. However, its X-ray flux at $T + 0.2$ d and $T + 0.6$ d

[1]In this work, we use vanilla ΛCDM cosmology with $H_0= 70$ km s^{-1} Mpc^{-1}, $\Omega_m= 0.3$, and $\Omega_\Lambda = 0.7$.

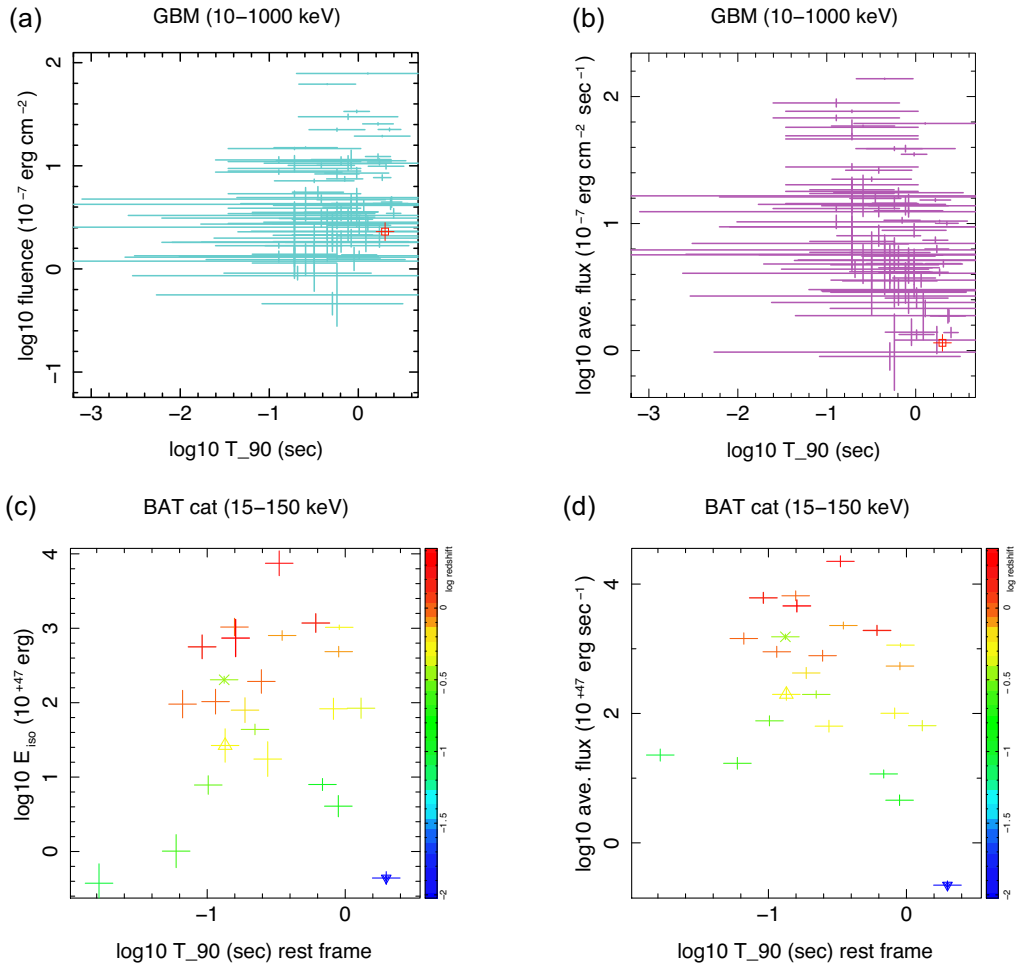

Figure 1. (a) Fluence as a function of T_{90} for short GRB's observed by the *Fermi*-GBM detector from Ref. Paciesa et al. (2012); (b) average flux determined by dividing fluence with T_{90} for the same data set as in plot (a). In these plots GRB 170817A is single out with a square symbol. (c) $E_{\rm iso}$ of short GRB's with known redshift in the *Swift*-BAT 15−150 keV energy band; (d) average flux of the same data as in (c). In (c) and (d) redshift is colour coded. The data used in these plots are taken from the *Swift* GRB on-line data base https://swift.gsfc.nasa.gov/archive/grb_table/ using as selection criteria $T_{90} \leq 2$ s. As GRB 170817A was not in the FoV of the *Swift*-BAT, in (c) and (d) we have used fluence measured in the *Fermi*-GBM 10 keV–2 MeV band. Thus, $E_{\rm iso}$ and average flux of GRB 170817A shown in these plots are upper limits and shown with an inverse triangle as the symbol of upper limit. Star symbol presents kilonova/GRB 130603B and up-right triangle shows GRB 160624A at z= 0.483, the only GRB with known redshift since 2015 September 1, considered as the beginning of the Advanced LIGO operation, which its GW could be a priori observed if it was at a lower redshift.

was smaller than upper limits reported by *Swift* and NuStar at these epochs for X-ray afterglow of GRB 170817A. Therefore, in contrast to suggestions in the literature, in absence of early observations we cannot conclude that GRB 170817A was unusually faint in X-ray at early times.

Another evidence for the presence of an early X-ray afterglow is the *Swift*-UVOT observations at $\sim T + 0.6$ d. They show a bright UV afterglow at this epoch. Giving the faintness and softness of the prompt γ-ray emission, the early X-ray afterglow of this GRB had to be equally soft and quickly decaying. This is consistent with the observation of a relatively bright early UV afterglow, which classifies this event as a blue kilonova at early times (Smartt et al. 2017; Covino et al. 2017; Cowperthwaite et al. 2017), see also Section 7 for more details.

Evidence of an X-ray counterpart was ultimately observed by *Chandra* observatory (Haggard et al. 2017; Troja et al. 2017) at T+ 9 d – only a lower limit flux of 2.7×10^{-15}erg s^{-1} cm^{-2} in 0.3–8 keV – and a measurement of slightly brighter flux of 3.5×10^{-15}erg s^{-1} cm^{-2} at $\sim T$+ 16 d. Similar late time brightening in X-ray and optical is observed in some short (Oates et al. 2009; Fong et al. 2013) and long (Cummings et al. 2006; De Pasquale et al. 2006) GRBs. They can be due to: MHD instabilities leading to increase in magnetic energy dissipation (Levinson & Begelman 2013; Bromberg & Tchekhovskoy 2016); external shock generated by the collision of a mildly relativistic thermal cocoon – ejected along with a relativistic GRB making jet – with the ISM or circumburst material (Nakar & Piran 2016; De Colle et al. 2017); or late outflows from an accretion disc (Murase et al. 2018). Therefore, it is not certain that late X-ray counterpart of GRBs is directly related to the relativistic jet, which is believed to generate the prompt gamma-ray, see also the commentary (Wijers 2018) about this issue.

For comparison, at T + 9 d and T+ 16 d the X-ray flux of GRB 111020A in 0.3–10 keV band was $\sim 8 \times 10^{-15}$erg s^{-1} cm^{-2} and $\sim 5 \times 10^{-15}$erg s^{-1} cm^{-2}, respectively. Considering the lower prompt gamma-ray flux of GRB 170817A, the above fluxes are proportionally similar to the Chandra observations of the late afterglow of GRB 170817A. However, Chandra upper limit at $\sim T$+ 2 d is much smaller than the flux of GRB 111020A at the

same epoch. None the less, it is consistent with much steeper decay slope observed in other short GRBs, notably kilonova/GRB 130603B.

In conclusion, taking into account the faintness of the prompt gamma-ray emission of GRB 170817A, its X-ray afterglow did not probably seem too unusual if it had been observed a few hundreds of seconds after the *Fermi*-GBM trigger.

3 PLAUSIBILITY OF AN OFF-AXIS OBSERVATION

One of the explanation for the faintness of GRB 170817A is its off-axis view. Here, we argue that based on statistical arguments and properties of other GRBs, it seems unlikely that the weakness of this GRB can be fully explained by geometry and viewing angle.

A far observer receives radiation of a relativistic emitter only from a cone around the source velocity direction with half-opening angle of $\theta = \sin^{-1}(1/\Gamma) \approx 1/\Gamma$ for $\Gamma \gg 1$, where Γ is Lorentz factor of emitter in the rest frame of observer (Rybicki & Lightman 2004). Lorentz factor of GRB jets are estimated to be $\Gamma \sim \mathcal{O}(100)$, see e.g. Zhang & Qin (2005), Zhao, Li & Bai (2010), and Evans et al. (2011). Even in GRB models in which the prompt emission is assumed to be produced by a magnetically dominated Poynting flow (Lyutikov & Blandford 2003; Zhang & Yan 2011; Nakar & Piran 2016), the Lorentz factor must be $\sim \mathcal{O}(10)$. Therefore, as long as the opening angle of the jet $\theta_j > [\sin^{-1}(1/\Gamma) \lesssim 6^\circ$ for $\Gamma \gtrsim \mathcal{O}(10)]$, the viewing can be considered as on-axis, unless the jet is strongly structured and its Lorentz factor at high latitudes is much smaller than on the jet axis.

According to numerical simulations of BNS merger (Hotokezaka et al. 2011; Rezzolla et al. 2011; Kiuchi et al. 2014; Dionysopoulou, Alic & Rezzolla 2015; Kawamura et al. 2016; Ruiz et al. 2016) the ejecta leading to a relativistic jet is poleward and has a half-opening angle of $\lesssim 30^\circ$. This is much larger than minimum θ_j discussed above. However, it is expected that the ultra-relativistic component of ejecta have a smaller opening angle (Tchekhovskoy, McKinney & Narayan 2008; Komissarov et al. 2009). Therefore, a priori the probability of off-axis view of short GRBs is much larger than on-axis. This implies unrealistically large number of compact object mergers, necessity for larger emission efficiency, and larger number of short bursts similar to GRB 170817, which is in contradiction with observations.

The solution for this conundrum, suggested long time ago, is the precession of compact objects orbits, specially during merger (Blackman, Yi & Field 1996; Ogilvie & Dubus 2001; Link 2002; Fargion 2005; Foucart et al. 2016). In addition, precession of the progenitors of GRBs may explain some of substructures in their light curves (Blackman et al. 1996; Fargion 2005; Ziaeepour & Gardner 2011). Precession frequencies as fast as $\mathcal{O}(100)$ Hz are expected during BNS merger (Morsink & Stella 1999). Moreover, GRMHD simulations of jet formation (Tchekhovskoy et al. 2008; Komissarov et al. 2009) show that the maximum Lorentz factor is attained in the middle or close to the outer part of jet funnel rather than on its rotation axis. Therefore, even in absence of precession in the central object, its rotation alone is enough for inducing a precession in the relativistic jet.

In presence of a precession with maximum angle θ_p, the sky surface covered by the jet is $4\pi|\cos(\theta_p + \theta_j) - \cos(\max[0, |\theta_p - \theta_j|])|$ rather than $4\pi(1 - \cos\theta_j)$ for a non-precessing jet. This relation is completely geometric and independent of the Lorentz factor of the jet, in contrast to opening angle, which may intrinsically depend on the Lorentz factor.[2] Without precession the probability that the line of sight fall outside the jet funnel is $P_{\rm out} = \cos\theta_j > 0.9$ for $\theta_j < 25^\circ$, whereas in presence of precession by a comparable amount, i.e. $\theta_p \sim 25^\circ$, the probability will be reduced to $P_{\rm out} = 0.36$. Thus, in absence of precession, if GW/GRB 170817 were an off-axis event with our line of sight passing close to outer boundary of a structured jet or a cocoon with a half-opening angle $\lesssim 25^\circ$, statistically speaking LIGO had to have observed $\sim$9 similar events without a GRB counterpart, because in 9 out of 10 events our line of sight would not intercept emission cone and we would not receive high energy synchrotron photons.

When the line of sight is outside the jet funnel, the observer only receive scattered photons, which their flux and energy would be much smaller than the primary synchrotron emission. Notably, Compton scattering of photons by electrons increases the flux at energies well below the synchrotron peak, see simulation of Ziaeepour & Gardner (2011) and Section 4. The peak energy of GRB 170817A is only $\sim$0.2−0.3 dex lower than other short GRBs, such as kilonova/GRB 130603B, and it is unlikely to be completely due to scattering of primary photons. Indeed, some of the analyses of late afterglow observations rule out off-axis model, see Section 7.1 for more details.

Obviously, based on the above statistical argument alone and observation of just one GW and GRB from a BNS merger it is not possible to rule out an off-axis prompt emission from GRB 170817A. None the less, it encourages us to consider the possibility that orders of magnitude faintness of this burst have an intrinsic origin.

4 PROMPT EMISSION MODEL

To understand properties of a relativistic jet or a cocoon, which might have generated such an unusual GRB, we use the phenomenological model and corresponding simulation code described in Ziaeepour (2009) and Ziaeepour & Gardner (2011). In this model the GRB prompt emission is produced by synchrotron/self-Compton processes in a dynamically active region at the head front of shocks between density shells inside a relativistic cylindrical jet. In addition to the magnetic field generated by *Fermi* processes in the active region, the model and corresponding simulation code can include an external magnetic field precessing with respect to the jet axis. The origin of such a field is irrelevant for the model. It can be a precessing Poynting flow or the magnetic field of a precessing central object, which after releasing the ejecta precesses with respect to the latter.

An essential aspect of this model, which distinguishes it from other phenomenological GRB formulations, is the evolution of parameters with time. In addition, simulation of each burst consists of a few time intervals – *regimes*. Each regime corresponds to an evolution rule (model) for phenomenological quantities such as fraction of energy transferred to fields and its variation; variation of the thickness of synchrotron/self-Compton emitting *active* region; etc. Division of simulated bursts to these intervals allows to change parameters and phenomenological evolution rules which are kept constant during one time interval. Continuity conditions implemented in the simulation code guarantees the continuity of physical

[2]Opening and precession angles θ_j and θ_p, respectively, are defined for an observer at the centre of progenitor. We remind that a far observer cannot measure the opening angle if $\theta_j > \sin^{-1}(1/\Gamma)$ and the jet axis does not precess.

Table 1. Parameters of the phenomenological prompt model.

Model (mod.)	Model for evolution of active region with distance from central engine; see AppendixA, and Ziaeepour (2009) and Ziaeepour & Gardner (2011) for more details.
r_0 (cm)	Initial distance of shock front from central engine.
Δr_0	Initial (or final, depending on the model) thickness of active region.
p	Slope of power-law spectrum for accelerated electrons; see equation 3.8 of Ziaeepour & Gardner (2011).
p_1, p_2	Slopes of double power-law spectrum for accelerated electrons; see equation 3.14 of Ziaeepour & Gardner (2011).
$\gamma_{\rm cut}$	Cut-off Lorentz factor in power law with exponential cutoff spectrum for accelerated electrons; see equation 3.11 of Ziaeepour & Gardner (2011).
γ_0'	Initial Lorentz factor of fast shell with respect to slow shell.
τ	Index in the model defined in equation 3.28 of Ziaeepour & Gardner (2011).
δ	Index in the model defined in equation 3.29 of Ziaeepour & Gardner (2011).
$Y_{\rm e}$	Electron yield defined as the ratio of electron (or proton) number density to baryon number density.
$\epsilon_{\rm e}$	Fraction of the kinetic energy of falling baryons of fast shell transferred to leptons in the slow shell (defined in the slow shell frame).
$\alpha_{\rm e}$	Power index of ϵ_e as a function of r.
$\epsilon_{\rm B}$	Fraction of baryons kinetic energy transferred to induced magnetic field in the active region.
$\alpha_{\rm B}$	Power index of $\epsilon_{\rm B}$ as a function of r.
N'	Baryon number density of slow shell.
κ	Power-law index for N' dependence on r'.
$n_{\rm c}'$	Column density of fast shell at r_0'.
Γ	Lorentz factor of slow shell with respect to far observer.
$\|B\|$	Magnetic flux at r_0.
f	Precession frequency of external field with respect to the jet.
α_x	Power-law index of external magnetic field as a function of r.
φ	Initial phase of precession, see Ziaeepour & Gardner (2011) for full description.

(1) The phenomenological model discussed in Ziaeepour (2009) and its simulation (Ziaeepour & Gardner 2011) depends only on the combination $Y_{\rm e}\epsilon_{\rm e}$. For this reason only the value of this combination is given for simulations.
(2) The model neglects variation of physical properties along the jet or active region. They only depend on the average distance from centre r, that is $r - r_0 \propto t - t_0$.
(3) Quantities with prime are defined with respect to rest frame of slow shell, and without prime with respect to central object, which is assumed to be at rest with respect to a far observer. Power indices do not follow this rule.

quantities between this time intervals, and adjustment of ensemble of parameters and intervals leads to light curves and spectra which well reproduce properties of real GRBs. In addition, implementation of some of discoveries of particle in cell (PIC) simulations, such as the small thickness of layer containing high energy electrons responsible for inverse Compton scattering of photons (Spitkovsky 2008; Murphy, Dieckmann & O'C Drury 2010; Sironi & Spitkovsky 2011a,b), lead to more realistic simulations.

Table 1 summarizes parameters of this model. Despite their long list, simulations of typical long and short GRBs in Ziaeepour & Gardner (2011) show that the range of values which lead to realistic bursts are fairly restricted. In this section we use this model to simulate the prompt emission of GRB 170817A and compare its properties with those of other short bursts, in particular GRB 130603B, which thanks to its brightness is extensively observed (Melandri et al. 2013) and classified as a kilonova (Berger et al. 2013; Tanvir et al. 2013).

4.1 Parameter selection

Because of large number of parameters in the phenomenological model, in order to find best fits to the data we restricted our search in the parameter space to most important characteristics, namely: r_0, p, $\gamma_{\rm cut}$, γ_0', Γ, $Y_{\rm e}\epsilon_{\rm e}$, $\epsilon_{\rm B}$, N', $n_{\rm c}'$, and $|B|$. Other parameters are fixed to values suitable for simulation of short GRBs with more typical characteristics, see Ziaeepour & Gardner (2011) for some examples.

Beginning with a choice for Γ, which determines kinematic of the ejecta, we changed the value of other parameters such that an acceptable fit to the data be found. We divide simulations according to the initial Lorentz factor of slow shell (bulk) Γ to three categories:

On-axis ultra-relativistic jet with $\Gamma \sim \mathcal{O}(100)$ (Zhang & Qin 2005; Zhao et al. 2010; Evans et al. 2011), see also simulations in Ziaeepour & Gardner (2011);

Off-axis structured relativistic jet with $\Gamma \sim \mathcal{O}(10)$ (Pian et al. 2017; Troja et al. 2017);

Mildly relativistic cocoon with $\Gamma \sim \mathcal{O}(1)$ (Nakar & Sari 2012; Nakar & Piran 2016; Gottlieb et al. 2017; Kasliwal et al. 2017a; Kathirgamaraju et al. 2018).
unnumlist

We remind that here *cocoon* means a mildly relativistic, mildly collimated outflow with a Lorentz factor of $\sim$2−3. It should not be confused with cocoon breakout model. We should also emphasize that as the exploration of parameter space was not systematic, the value of parameters in models with best fits to the data should be considered as approximation rather than exact. Another important issue, specially when considering the best models, is the fact that parameters of the phenomenological model studied in Ziaeepour (2009) are not completely independent. For instance, based on physical principles it is expected that fraction of kinetic energy transferred to induced electric and magnetic fields depend on the strength of the shock, which is determined by the density difference of colliding shells and their relative Lorentz factor. But there is no simple formulation for these dependencies, and they could not be considered in the phenomenological model. We leave further discussion of this issue to the next section, where we assess plausibility of selected simulations.

4.2 Simulation of GRB 170817A

Fig. 2 shows light curves of the four best simulated bursts according to their chi-square fit in 10 keV–1 MeV band along with the *Fermi*-

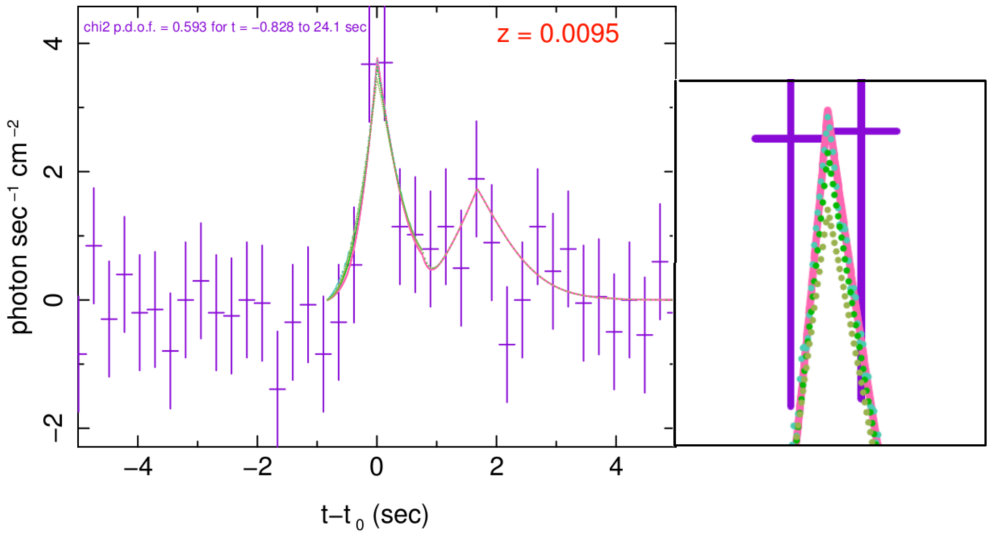

Figure 2. Light curves of the four best simulations in 10 keV–1 MeV. The data are from observations of *Fermi*-GBM (Goldstein et al. 2017). This plot shows that these simulations have very similar light curves. The inset is a zoom on the first peak and shows the slight difference of the amplitude of the first peak in these models. The value of χ^2 is for the full line corresponding to model No. 2 in Table 2 for the first peak and model No. 3 for the second peak. Other curves (dotted lines) correspond to model No. 1 with and without an external magnetic field (blue and dark green curves, respectively), and an off-axis model with all parameters the same as model No. 2, except column density of ejecta which is $n'_c = 5 \times 10^{25}$ cm^{-2} (light green). The value of χ^2 per degree of freedom of the first two simulations are about 0.02 larger than model No. 2 and that of the last model is ∼0.03 larger.

GBM data. The two peaks in the observed light curve are simulated separately and adjusted in time such that the sum of two peaks minimize χ^2-fit to the data. Fig. 3 shows light curves in narrower bands for each peak and Fig. 4 their spectra. Table 2 shows the value of parameters for these simulations. Table 3 shows the value of parameters we have explored to find best fits to the data. They correspond to simulations which do not fit the data well. The last column of this table describes their deficiencies and Fig. 5 shows light curves and spectra of a sample of them. We use these results here and in Section 5 to assess how variation of parameters affects properties of simulated GRBs, and to which extent parameters are degenerate.

Similarity of light curves of simulations with best fits, despite large differences in some of their parameters, shows the degeneracy of parameters of the phenomenological model. None the less, fitting the spectrum of the first peak to data provides further selection criteria. We did not fit the simulated model to the spectrum of the second peak because the data in Goldstein et al. (2017) includes only two measured data points at lowest energies for this peak and other data points are observational limits. Fig. 4 shows spectra of four simulations which their light curves are shown in Fig. 2. From this figure it is evident that spectrum in Fig. 4(d) is a weaker fit to data than other models shown in this figure. It has a cumulative probability of random coincidence[3] of $P \approx 0.12$ for 10 degrees of freedom, where other three models have $P \approx \mathcal{O}(1) \times 10^{-3}$. Despite differences in goodness of fit, all these simulation are very similar to each others and to the data, and it is not possible to choose one of them as the best fit to the GBM data. However, the comparison of spectra in 4(a) and 4(b), which their only difference is an external magnetic field in the former, may be interpreted as the necessity of a mild magnetic field in addition to the field induced by *Fermi* processes in the shock front.

To better understand the correlation between parameters of the model, their degeneracies, and how they affect the main observables of GRB170817A, namely light curves and spectrum, Fig. 6 shows colour-coded χ^2 value of simulations presented in Tables 2 and 3 in 2D parameter planes for a subset of parameters of the phenomenological model, which are related to primary properties of the relativistic jet and vary significantly in our simulations. The plots in this figure show that despite small coverage of 2D parameter planes by our simulations, for each parameter both high and low values are sampled – except in case of n'_c for cocoon models, in which by definition the column density of outflow could not be larger than relativistic jets. We notice large parameter degeneracies between models with good light-curve fit, i.e. $\chi^2 < 1$, which is consistent with similarity of light curves in Fig. 2. By contrast, many models with very different spectral χ^2 fall on the same position in 2D parameter planes. Such behaviour is present in all the combination of parameters shown in Fig. 6 and means that the spectral behaviour depends on multiple parameters and cannot be well presented by a 2D parameter space.

4.3 Comparison with GRB 130603B

For the purpose of comparison the fourth model in Table 2 presents parameters of a simulation reproducing properties of the first peak of the bright short burst GRB 130603B, accompanied by a kilonova (Berger et al. 2013; Tanvir et al. 2013).[4] The simulated light curves and spectrum of this model are shown in Fig. 7. The difference between characteristics of this model and simulations of GRB

[3]Here, the cumulative probability is defined as $P(X < \chi^2_{\rm data})$, where X is a random variable with chi-square distribution and $N-1$ degrees of freedom; N is the number of data points; and $\chi^2_{\rm data}$ is the value of chi-square fit of data to model.

[4]This simulation must be considered only as a simulated burst *similar* to GRB 130603B because the parameter space was not extensively explored to find the best match. Notably, in contrast to GRB 170817A, no attempt was made to simulate the two peaks of this burst separately.

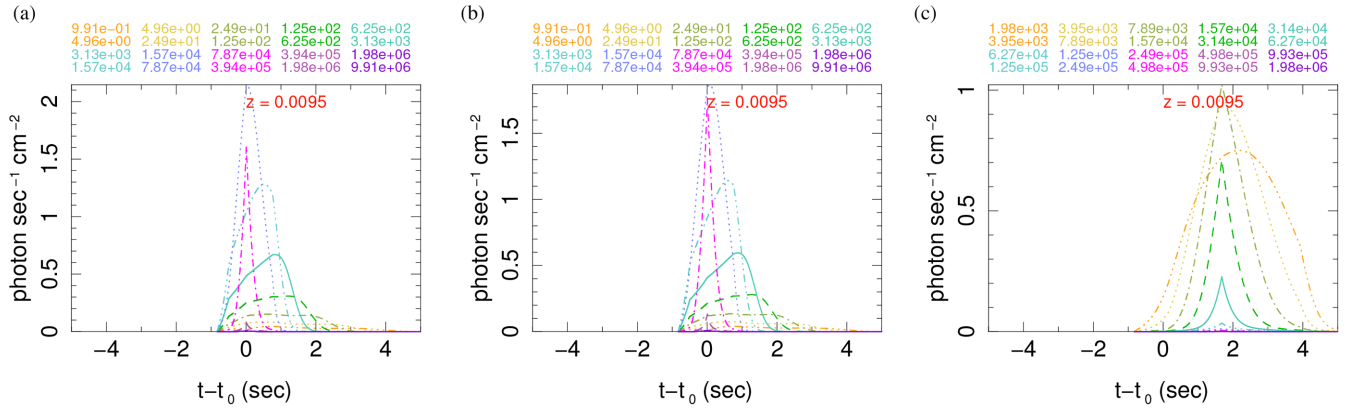

Figure 3. Light curves of simulated models in energy bands covered by *Fermi*-GBM and Integral SPI-ACS instruments: (a) simulation No. 2; (b) simulation No. 1 without external magnetic field; (c) second peak, that is simulation No. 3. All simulation numbers refer to Table 2. Minimum and maximum of each energy band in eV is written in the corresponding colour on the top of each plot. Notice that the second peak is simulated in lower energy bands than the first peak. The lag between highest energy bands is roughly zero and consistent with observation of short GRBs.

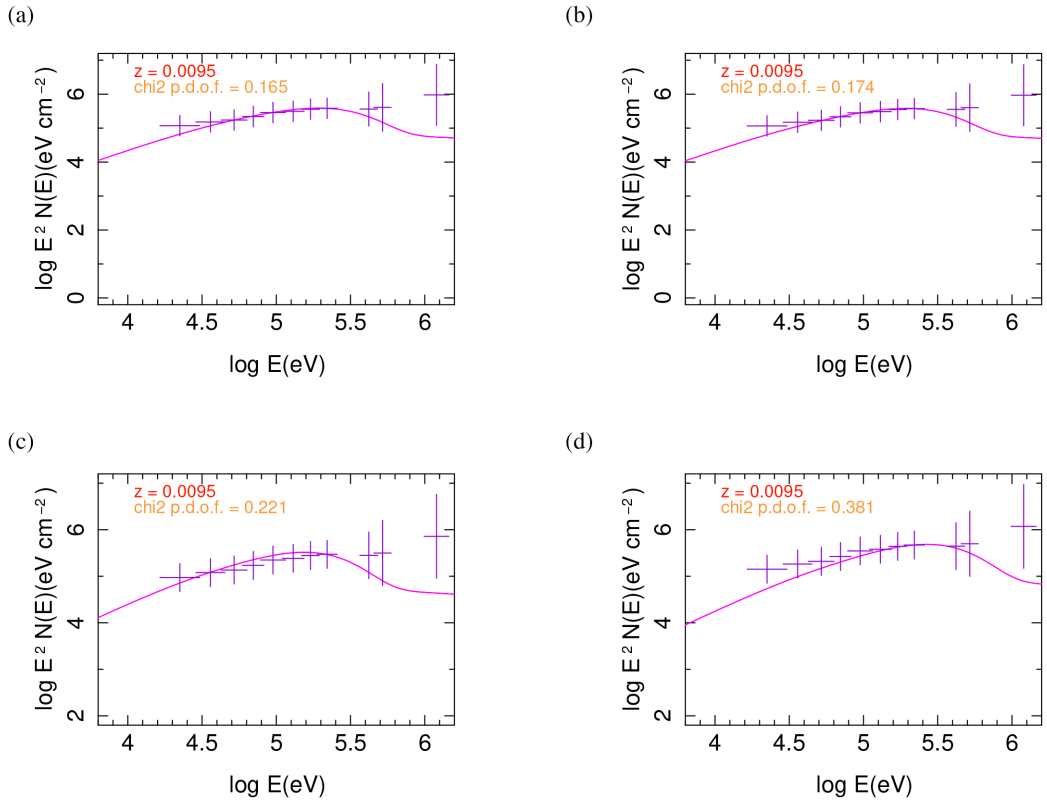

Figure 4. Spectra of simulated models fitted to *Fermi*-GBM data: (a) model No. 1; (b) model No. 1 without external magnetic field; (c) model No. 2; (d) a model with the same parameters as models No. 2 except for $n'_c = 5 \times 10^{25}$ cm^{-2}. As the published spectral data in Goldstein et al. (2017) is in count rate, after changing it to energy flux we used peak energy from Goldstein et al. (2017) to normalize data such that at $E = E_{\rm peak} = 215 \pm 54$ keV observed and simulated spectra have the same amplitude. For this reason, spectra of simulated models have much smaller χ^2 than their corresponding light curves. The data point with highest energy and uncertainty is considered to be an outlier and is not included in the calculation of χ^2 because it may affect fitting and lead to large deviation from true model, see e.g. Grubbs (1969).

170817A is remarkable: the jet extent is ∼20-folds (in comparison with model No. 1) or ∼40 folds (in comparison with model No. 2) larger; the slow shell is five times denser; fraction of kinetic energy transferred to electrons weighed by electron yield, that is $\epsilon_{\rm e} Y_{\rm e}$ is 2-folds larger than in model No. 1; bulk Lorentz factor of ejecta is larger by a factor of 5 (in comparison with model No. 1) and by a factor of 50 (in comparison to model No. 2); external magnetic field is ∼30 times stronger than models No. 1 and 2. These differences are easily noticeable in 2D parameter space plots in Fig. 6. We also notice that in comparison to data, simulation No. 4 in Table 2 somehow overestimates X-ray and soft gamma-ray emission. This may be due to the opacity of the high density jet for these soft photons and the absence of self-absorption in our code.

Table 2. Parameter set of simulated models.

No.	GRB/peak	Mod.	Γ	r_0 (cm)	$\frac{\Delta r_0}{r_0}$	$\left(\frac{r}{r_0}\right)_{\max}$	$p(p_1)$	p_2	$\gamma_{\rm cut}$	κ	γ'_0	τ	δ
1	GW/GRB	1	100	2×10^{10}	5×10^{-5}	1.5	2.5	–	10	0	1.5	–	1
	170817: first	0	–	–	–	1.5	–	–	10	0	–	0	–
	peak, rel.jet	2	–	–	–	1.5	–	–	10	0	–	–	3
		2	–	–	–	4	–	–	10	0	–	–	5
2	GW/GRB	1	10	2×10^{10}	5×10^{-5}	1.5	2.5	–	10	0	1.5	–	1
	170817: first	0	–	–	–	1.5	–	–	10	0	–	0	–
	peak, off-axis	2	–	–	–	1.5	–	–	10	0	–	–	3
		2	–	–	–	4	–	–	10	0	–	–	5
3	GW/GRB	1	30	6×10^{10}	5×10^{-5}	1.5	2.5	–	10	0	1.5	–	1
	170817: second	0	–	–	–	1.5	–	–	10	0	–	0	–
	peak	2	–	–	–	1.5	–	–	10	0	–	–	3
		2	–	–	–	4	–	–	10	0	–	–	5
4	GRB	3	500	8×10^{9}	5×10^{-3}	15	2.1	3	3	0	1.5	–	2
	130603B	2	–	–	–	15	–	3	3	0	–	–	3
		2	–	–	–	15	–	3	3	0	–	–	4

No.	GRB/peak	$\epsilon_{\rm B}$	$\alpha_{\rm B}$	$\epsilon_{\rm e}Y_{\rm e}$	$\alpha_{\rm e}$	N' (cm^{-3})	$n'_{\rm c}$ (cm^{-2})	$\lvert B\rvert$ (kG)	f (Hz)	α_x	φ (rad)
1	GW/GRB	10^{-4}	-1	0.01	-1	2×10^{14}	10^{25}	0.8	500	–	–
	170817: first	–	-2	–	-2	–	–	–	–	1	–
	peak, rel.jet	–	2	–	2	–	–	–	–	2	–
		–	4	–	4	–	–	–	–	3	–
2	GW/GRB	10^{-4}	-1	0.03	-1	2×10^{14}	5×10^{24}	0.5	500	1	–
	170817: first	–	-2	–	-2	–	–	–	–	1	–
	peak, off-axis	–	2	–	2	–	–	–	–	2	–
		–	4	–	4	–	–	–	–	3	–
3	GW/GRB	10^{-4}	-1	0.01	-1	2×10^{13}	5×10^{23}	0	–	–	–
	170817: second	–	-2	–	-2	–	–	–	–	–	–
	peak	–	2	–	2	–	–	–	–	–	–
		–	4	–	4	–	–	–	–	–	–
4	GRB	10^{-4}	-2	0.02	-2	10^{15}	2×10^{26}	26	500	1	0
	130603B	–	2	–	2	–	–	–	–	1	0
		–	3	–	2	–	–	–	–	1	0

(1) Each data line corresponds to one simulated regime, during which quantities listed here remain constant or evolve dynamically according to fixed rules. A full simulation of a burst usually includes multiple regimes (at least two).
(2) Horizontal black lines separate time intervals (regimes) of independent simulations identified by the number shown in the first column.
(3) A dash as value for a parameter presents one of the following cases: it is irrelevant for the model; it is evolved from its initial value according to an evolution equations described in Ziaeepour (2009) and Ziaeepour & Gardner (2011); or it is kept constant during all regimes.

To see whether degeneracy in the value of Lorentz factor, which we found in simulations of GRB 170817A, are also present in harder and brighter bursts, we attempted to simulate GRB 130603B with a Lorentz factor of 50. We could not find any model with a flux as high as what was observed for this burst, a peak energy of ∼900 keV in the rest frame of the burst, and $Y_{\rm e}\epsilon_{\rm e} < 0.1$, which is motivated by PIC simulations (Spitkovsky 2008; Sironi & Spitkovsky 2011a,b). For $\epsilon_{\rm e}Y_{\rm e} \sim 0.1$ the peak energy is not too far from observed value. However, with an electron yield $Y_{\rm e} \lesssim 0.3$ expected in kilonova ejecta, the fraction of kinetic energy transferred to electrons must be ∼0.3, which is too large to be inconsistent with prediction of PIC simulations. Therefore, it seems that in what concerns the apparent degeneracy of models with $\Gamma \sim 100$ and $\Gamma \sim 10$, GRB 170817 is an exception.

The fluence of GRB 130603B in Konus-wind 20 keV–10 MeV energy band was $E_{\rm iso} = (2.1 \pm 0.2) \times 10^{51}$ ergs (Frederiks et al. 2013), i.e. $\gtrsim 10^4$ times larger than in GRB 170817A. The peak energy of $E_{\rm peak} \approx 900 \pm 100$ keV in the rest frame of this burst was ≈4 times higher than the latter. We should also remind that $E_{\rm iso}$ and $E_{\rm peak}$ of GRB 130603B were not exceptionally high and present typical values for short bursts, see Fig. 1 and e.g. Paciesa et al. (2012). Therefore, we conclude that lower densities of shells and smaller jet extend of GRB 170817 with respect to more typical bursts were responsible for unusual properties of this GRB.

Finally, because no observation in low energies from trigger time up to few tens of thousands of seconds is available, we did not try to simulate afterglows of GRB 170817. Later afterglows are expected to be superimposed with emission from slow components such as wind and ejecta from a disc, and do not directly present properties of emission generated by external shocks during passage of the prompt relativistic jet through circumburst environment. In absence of any early data, it would be meaningless and confusing to make conclusions about an unobserved emission only based on theoretical assumptions. None the less, modelling of late afterglows is by itself interesting, specially because this burst is the first short GRB with long and extended observation of its late afterglow. It

Table 3. Simulations with altered parameters with respect to those presenting best fits to GRB 170817A data.

No.	Γ	r_0 (cm)	$p(p_1, p_2)$	$\gamma_{\rm cut}$	γ'_0	$\epsilon_{\rm B}$	$Y_{\rm e}\epsilon_{\rm e}$	N' (cm^{-3})	$n'_{\rm c}$ (cm^{-2})	$\lvert B\rvert$ (kG)	$\chi^2_{\rm lc}$ p.d.o.f.	$\chi^2_{\rm spect}$ p.d.o.f.	Deficiencies
Relativistic jet models													
1	400	2×10^{10}	1.5	200	1.5	10^{-4}	0.02	5×10^{14}	5×10^{25}	1	429.9	1.49	Too hard; too bright
2	100	2×10^{10}	1.5	200	1.5	10^{-4}	0.02	5×10^{14}	5×10^{26}	1	311.9	0.58	Too bright; positive spectral index at high energies
3	200	2×10^{10}	1.5	200	1.5	10^{-4}	0.02	5×10^{14}	5×10^{26}	0	284.6	1.07	Too hard; too bright
4	100	2×10^{10}	2.2	10	1.5	10^{-4}	0.01	5×10^{14}	5×10^{26}	1	464.4	0.8	Too soft; too bright
6	100	2×10^{10}	2.5	10	1.5	10^{-4}	0.01	5×10^{14}	5×10^{25}	1	7.335	0.525	Slightly too hard; too bright
7	100	2×10^{10}	2.5	10	1.5	10^{-4}	0.01	5×10^{14}	3×10^{25}	1	7.694	0.405	Too bright
8	100	2×10^{10}	2.5	10	1.5	10^{-4}	0.01	10^{13}	5×10^{25}	1	1.382	0.568	Slightly too soft; too faint
9	100	2×10^{10}	2.5	10	1.5	10^{-4}	0.01	2×10^{14}	5×10^{25}	1	0.642	0.439	Slightly too hard
10	100	2×10^{10}	2.5	10	1.5	10^{-4}	0.01	2×10^{14}	5×10^{25}	1 (f= 5 Hz)	0.644	0.524	Slightly too hard
11	100	2×10^{10}	2.5	10	1.5	10^{-4}	0.01	2×10^{14}	10^{25}	1	1.903	1.68	Peak too soft; too bright in soft γ-ray energies
12	100	2×10^{10}	3	10	1.5	10^{-4}	0.02	2×10^{14}	5×10^{25}	0	1.094	2.81	Too hard; too faint
13	150	2×10^{10}	2.5	10	1.5	10^{-4}	0.02	2×10^{14}	10^{26}	1	0.697	1.02	Too hard
Off-axis models													
15	10	10^{12}	2.5	10	1.5	10^{-4}	0.1	2×10^{14}	5×10^{25}	0	6×10^{6}	–	Too bright; too long
16	10	2×10^{10}	2.5	10	1.5	10^{-4}	0.01	2×10^{14}	5×10^{25}	0	1.110	5.43	Too soft
17	10	2×10^{10}	2.5	10	1.5	10^{-4}	0.05	2×10^{14}	5×10^{25}	0	0.675	1.4	too faint, too hard
Cocoon models													
18	3	2×10^{11}	2.5	10	1.5	10^{-6}	0.03	2×10^{15}	5×10^{24}	26	–[a]	–[a]	Too bright; too soft; too long
19	3	2×10^{11}	2.5	10	1.5	10^{-6}	0.03	2×10^{15}	5×10^{24}	26	–[a]	–[a]	Too soft; too long
20	3	2×10^{11}	2.5	10	1.5	10^{-6}	0.03	2×10^{15}	5×10^{24}	2.6	–[a]	–[a]	Too soft; too long
21	3	2×10^{11}	2.5	10	1.5	10^{-4}	0.01	2×10^{15}	5×10^{24}	2.6	–	–	Too bright; too soft; too long
22	3	2×10^{11}	2.5	10	1.5	10^{-4}	0.01	2×10^{15}	5×10^{24}	26	–	–	Too bright; too soft; too long
23	3	2×10^{11}	2.5	10	1.5	10^{-4}	0.01	2×10^{13}	5×10^{24}	2.6	–	–	Too soft; too long

Note. Values in this table correspond to initial value of parameters in the first regime of each simulation. Other parameters and regimes are similar to models given in Table 2 and are not shown here for the sake of clarity.
[a] Peak of light curves out of observation time.

may provide valuable information about the state of slow ejecta and their evolution with time. This a work in progress and will be reported elsewhere.

In conclusion, the interest of using the same phenomenological model for modelling multiple bursts is that one can compare their parameters and properties in the same theoretical setup. This allows to estimate the effect of variation of physical properties of jet and environment from burst to burst, and conclusions should be less affected by theoretical uncertainties than absolute value of parameters.

5 INTERPRETATION OF PROMPT EMISSION SIMULATIONS

In Section 4 we divided candidate models and corresponding simulations of GRB 170817A into three categories according to their Lorentz factor, namely: mildly relativistic cocoon, off-axis view of a structured jet, and on-axis ultra-relativistic jet. This classification is motivated by short GRB models and suggestions in the literature for the origin of this unusually soft and faint burst (Evans et al. 2017; Goldstein et al. 2017; Kasliwal et al. 2017a; Pian et al. 2017). In this section we discuss the plausibility of these hypotheses, based on the results of simulations presented in Section 4.2.

5.1 Mildly relativistic cocoon

From results presented in Fig. 5 and Table 3, and discussions in Section 4.2, it is clear that mildly relativistic cocoons with characteristics similar to what is suggested in Kasliwal et al. (2017a) cannot reproduce observed properties of GRB 170817A prompt emission. All the simulations with $\Gamma \sim 2-3$ and prompt shock at a distance of $\mathcal{O}(1)\times10^{11}$cm are too soft and have a duration $\gtrsim$10 s, too long to be consistent with observations of *Fermi*-GBM and Konus-Wind. However, we remind that this conclusion is for synchrotron/self-Compton emission generated by internal shocks in the cocoon. There is another version of cocoon model which associates the soft emission to breakout of the jet or outflow. This mechanism cannot be directly studied with our simulation code. None the less, we in the next subsection we use phenomenological formulation of Nakar & Sari (2012) and Kasliwal et al. (2017a) to assess the plausibility of this model as an explanation for unusual characteristics of GRB 170817A.

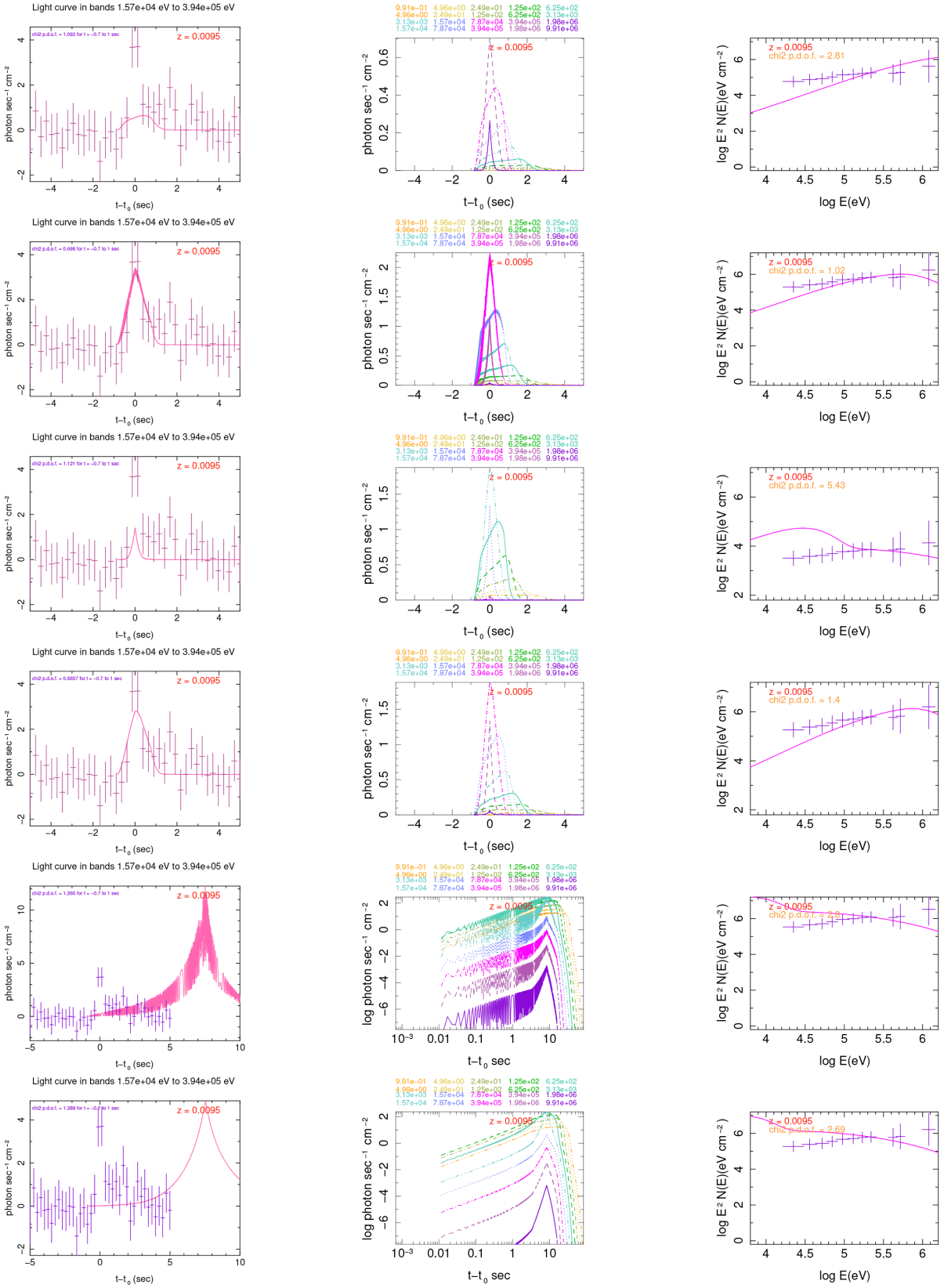

Figure 5. Broad-band (left) and narrow-band (middle) light curves, and spectra (right) of a sample of simulations which are not good fit to the first peak of GRB 170817A. From top to bottom they correspond to simulations: 11, 12, 16, 17, 19, and 20 in Table 3. Rapid variation is visible in the light curves when the precessing magnetic field is strong and precession is fast. They cannot be distinguished from shot noise if precession period is shorter than time resolution or binning of data. For the sake of clarity the narrow-band light curves of the last two models are shown in logarithmic scale. We remind that GBM spectral data are normalized such that it has the same amplitude as simulations at $E = E_{\rm peak} = 215 \pm 54\,{\rm keV}$

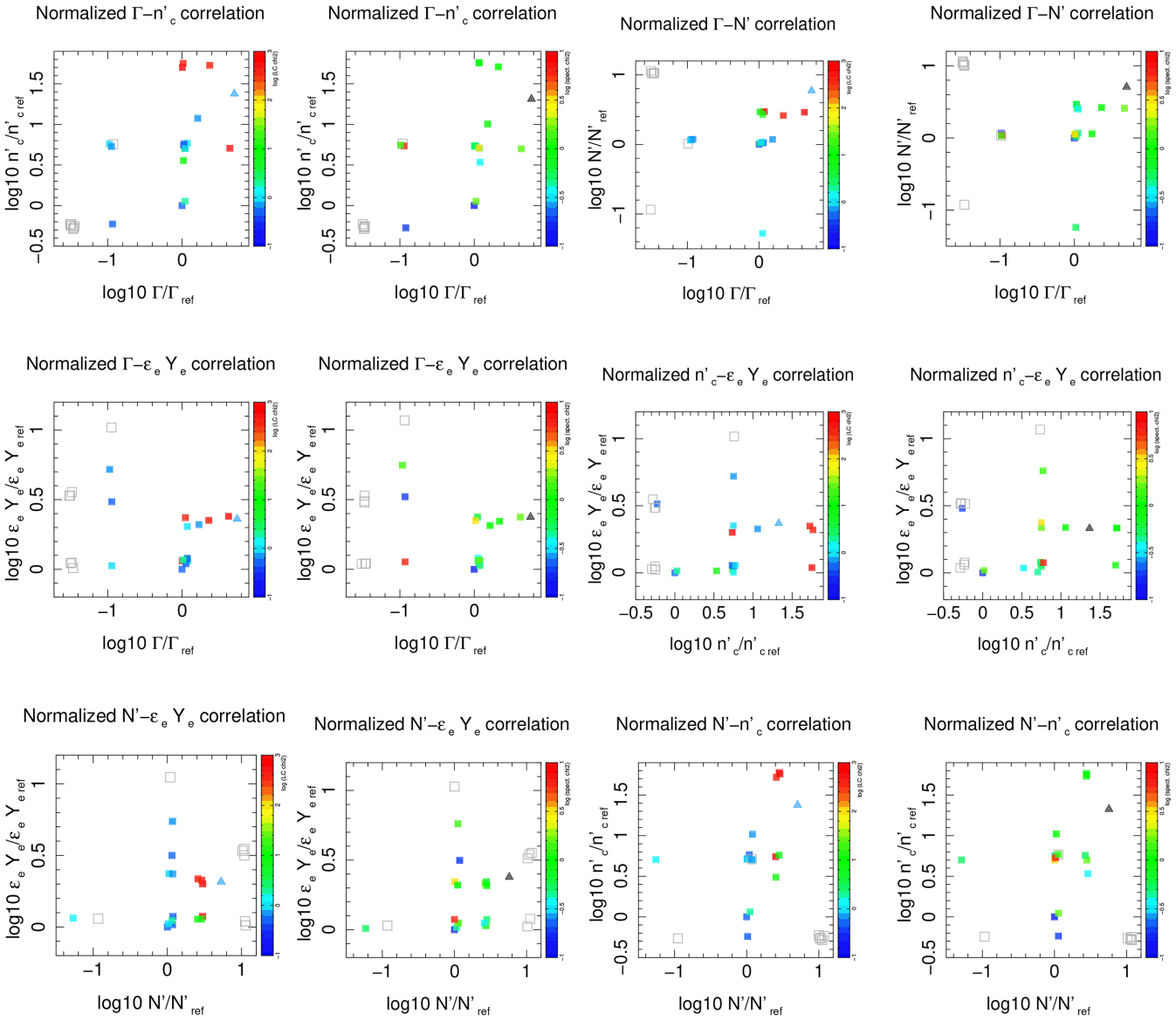

Figure 6. Color-coded χ^2 per degree of freedom for simulations presented in Tables 2 and 3 in 2D parameter planes. To make the comparison between models easier, all parameters are normalized by the corresponding value in simulation No. 1 in Table 2. From left, in odd columns χ^2 is obtained by fitting broad-band light curve to GBM data, and in even columns from fitting the spectrum. Open squares present simulations with χ^2 larger than maximum value shown in the colour coded scale. Triangle symbol presents simulation No. 4 in Table 2 which its properties are similar to GRB 130603B. Only data of the first peak are used to estimate χ^2 of this simulation. No broad-band spectral data for this burst are available and the absence of χ^2 is shown by using colour black for triangle symbols in the plots. To prevent overlap of symbols they are slightly and randomly shifted in both directions. The shift is much smaller than variation of parameters among different simulations and very compact clumps of symbols mean the same value for two parameters in the corresponding simulations. When one of the plotted parameters is Lorentz factor, three groups of simulations with $\Gamma \sim \mathcal{O}(1)$ (cocoon), $\Gamma \sim \mathcal{O}(10)$ (off-axis), $\Gamma \sim \mathcal{O}(100)$ (ultra-relativistic) are distinguishable.

5.1.1 Cocoon breakout

Cocoon breakout model for faint GRBs (Nakar & Sari 2012) assumes that the relativistic jet is chocked by thick envelop of a collapsing star or dense slow ejecta surrounding a binary merger. The intervening material traps radiation generated by shocks and other processes until its expansion reduce the opacity and release the trapped photons. Due to multiple scattering during their confinement, photons become either fully or partially thermalized and their spectrum become softer. In this respect, this model is a low energy analogue of standard fireball mechanism, in which the gamma-ray in GRBs is assumed to be due to $e^{\pm}$ annihilation when a leptonic plasma become optically thin. The spectrum of GRBs in fireball model contains a dominant thermal (blackbody) component (Rees & Mészáros 2005; Pe'er, Mészáros & Rees 2006; Ioka et al. 2007).

In what concerns GRB 170817A, its spectrum, specially the first peak, is power law with exponential cutoff (Goldstein et al. 2017), thus consistent with a synchrotron rather than thermal emission. Indeed, observations show that synchrotron emission from relativistic shocks is the main contributor in prompt gamma-ray emission of almost all GRBs, although in some bursts addition of a thermal component – from photospheric or slower outflows – may improve spectral fit, see e.g. Burgess et al. (2017).

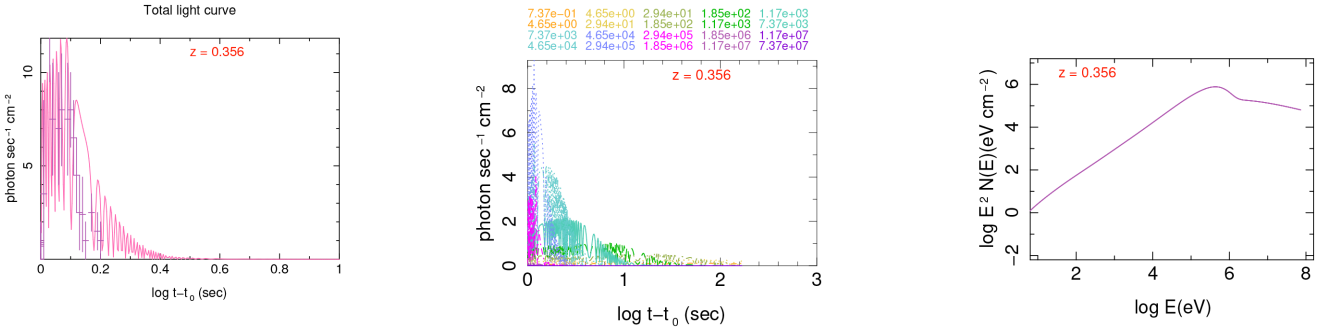

Figure 7. Broad-band (left) and narrow-band (middle) light curves and spectrum (right) of model No. 4 in Table 2, which is a good approximation for the first peak of GRB 130603B. Data points are from *Swift*-BAT observations in 15–350 keV band. The peak energy of the spectrum is very close to $E_{\rm peak} = 660 \pm 100$ keV of the short GRB 130603B observed by Konus-Wind (Golenetskii et al. 2013). No broad-band spectral data are publicly available for this burst to compare with simulated spectrum.

The semithermal spectrum of cocoon breakout is presented by an effective temperature $T_{\rm bo}$ and a bolometric fluence $E_{\rm bo}$. Duration of emission $t_{\rm bo}$ is a function of latter quantities and estimated as (Nakar & Sari 2012; Kasliwal et al. 2017a):

$$t_{\rm bo} \sim 1\,{\rm s}\left(\frac{E_{\rm bo}}{10^{46}\,{\rm erg}}\right)^{\frac{1}{2}}\left(\frac{T_{\rm bo}}{150\,{\rm keV}}\right)^{-\frac{9+\sqrt{3}}{4}}. \quad (1)$$

Assuming that in GRB 170817A $T_{\rm bo} \sim E_{\rm peak} \sim 230$ keV, with a bolometric fluence of $E_{\rm bo} \sim 10^{47}$ ergs, we obtain $t_{\rm bo} \sim 0.8$ s $\ll$ 2 s duration of this burst. A lower $T_{\rm bo}$ can increase duration of emission, but will have problem to explain detection of high energy photons up to $\gtrsim$1 MeV.[5] For having such a high effective temperature, the terminal Lorentz factor before breakout must be $\Gamma_f \sim T_{\rm bo}/50$ keV ~ 5 (Nakar & Sari 2012), which is larger than the value used in the literature and in our cocoon simulations. Moreover, using the relation between final Lorentz factor and star radius – or in the case of short bursts distance of circum-merger material from centre, $\Gamma_f \sim 30 M_5^{0.14} R_5^{-0.27}$, where M_5 is the mass of material in units of $5\,{\rm M}_\odot$ and R_5 is distance from centre in units of $5\,{\rm R}_\odot$ (Nakar & Sari 2012), we find a distance of $\sim 60\,{\rm R}_\odot \sim 4 \times 10^{12}$ cm for $M_5 \sim 0.006 \sim 0.03\,{\rm M}_\odot$, which corresponds to estimated mass of polar outflow from kilonova AT 2017 gfo (Arcav et al. 2017; Kasen et al. 2017; Smartt et al. 2017). If the material is ejected at the time of merger collapse to BH, then there had to be $\lesssim$100 s of delay between the end of GW and detection of GRB. This is much longer than the observed delay of $\sim$1.7 s (Goldstein et al. 2017; Savchenko et al. 2017). In conclusion, breakout of a mildly relativistic cocoon may explain or contribute in the early low energy emissions, but cannot explain the observed prompt gamma-ray.

5.2 Off-axis jet

Table 2 shows that if $\Gamma \sim 10$, other parameters, in particular $\epsilon_{\rm e} Y_{\rm e}$, can be adjusted to obtain a burst with properties of GRB 170817A prompt emission. If this apparent low Lorentz factor is due to an off-axis view of the ultra-relativistic jet, the relation between emitted and received power (Rybicki & Lightman 2004):

$$\frac{\frac{{\rm d}P_{\rm e}}{{\rm d}\omega {\rm d}\Omega}}{\frac{{\rm d}P_{\rm r}}{{\rm d}\omega {\rm d}\Omega}} = \frac{1}{\Gamma^2(1+\beta\cos\theta_v)}, \quad (2)$$

where θ_v is angle between a far observer and jet axis, shows that an off-axis view of the jet alone is not enough to explain the faintness of GRB 170817A. On the other hand, a structured jet by definition has lower Lorentz factor at high latitudes and may explain a softer and a few orders of magnitude smaller fluence of this burst in comparison to typical short bursts, shown in Fig. 1. However, in this case one expects significant brightening of the afterglow when the dissipation of energy through collision of the jet with circumburst material reduces beaming and makes the central region of the jet visible to a far off-axis observer (Lazzati et al. 2017a). Such a brightening is not observed for GRB 170817A, and as we discussed in Section 2.1 the slight late brightening in X-ray is not unique to this burst and has been seen in bright, presumably on-axis, bursts. For instance, in the case of GRB 130603B the brightening of the X-ray afterglow was observed at $\sim$10 d after prompt emission (Fong et al. 2013), which is roughly the same epoch as that of GRB 170817A. Therefore, we conclude that the late afterglow cannot be uniquely associated with interaction of the relativistic jet with circumburst material and its brightening due to the opening of an off-axis jet, as predicted by Lazzati et al. (2017a) formulation. Furthermore, the UV/optical/IR counterpart AT 2017 gfo indicates a dominantly thermal ejecta of mass $M_{\rm ejecta} \sim 0.03$–$0.05\,{\rm M}_\odot$ at $\sim T + 0.6 - T + 1.5$ d (Arcav et al. 2017; Pian et al. 2017; Smartt et al. 2017). A relativistic jet of mass $M_{\rm jet} \sim 10^{-6}\,{\rm M}_\odot$ (Evans et al. 2017; Kasliwal et al. 2017a) and its synchrotron/self-Compton emission cannot explain neither the observed flux nor the features seen in the low energy spectrum. Thus, additional ejecta components must be involved in the production of these emissions. Indeed, evidence for additional ejecta, such as an expanding thermal cocoon, expanding envelop, and/or evaporating disc are found in other GRBs too (Piro et al. 2014; Tanaka 2016).

The prompt gamma-ray emission cannot be due to scattered photons either. Fig. 8 shows the spectrum of scatted photons through Compton scattering by fast electrons for simulations No. 1 and 2 in Table 2. The shape of these spectra deviates significantly from observed spectrum. Notably, the dominant peak of Compton spectrum is at much lower energies and its amplitude is few orders of magnitude less than synchrotron emission for both high and low Γ simulations No. 1 and 2, respectively. Our simulation code does not include Compton scattering of photons by hadrons. However, simulations of this process (Asano, Inoue & Meszaros 2010; Murase et al. 2012) shows that similar to leptonic case its effect is dominant at high energy tail i.e. $E \gtrsim 1$ MeV and low energies, but not in 10^2–10^3keV energy band, which includes the peak energy of most

[5]Indeed, Kasliwal et al. (2017a) use $T_{\rm bo} \sim 150$ keV in their analysis to obtain a longer prompt emission. However, they do not present any comparison of their model with the *Fermi*-GBM or Integral-IBIS prompt gamma-ray data.

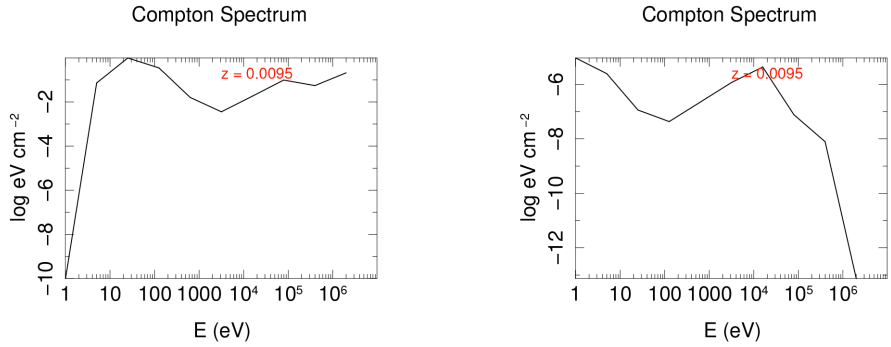

Figure 8. Spectrum of Compton scattering of photons by fast electrons in simulations No. 1 (left) and No. 2 (right).

short and long GRBs. In addition, no high energy excess, which could be associated with hadronic processes was detected in GRB 170817A. Therefore, we conclude that the prompt gamma-ray of this burst could not be due to scattered of higher energy photons from an off-axis jet.

Alternatively, the GRB forming jet of GW 170817 event might have intrinsically a low Lorentz factor of order $\Gamma \sim \mathcal{O}(10)$, rather than $\Gamma \sim \mathcal{O}(100)$ estimated for most short GRBs by the phenomenological model and simulations of Ziaeepour (2009) and Ziaeepour & Gardner (2011), see also parameters for GRB 130603B in Table 2, and estimation of Lorentz factor of GRBs in literature (Zhang & Qin 2005; Zhao et al. 2010; Evans et al. 2011; Ghisellini et al. 2012). Indeed, in Section 4 we reported simulations consistent with the first peak of GRB 170817A with both $\Gamma \sim 100$ and $\Gamma \sim 10$. However, Table 2 shows that to compensate for low Lorentz factor $\Gamma \sim 10$, the efficiency of energy transfer to electrons (more generally charged leptons) must be ∼3 times larger than simulations with $\Gamma \sim 100$. On the other hand, as we discussed in Section 4.3, according to our simulations the density of colliding shells in GRB 170817A were more than an order of magnitude smaller than e.g. GRB 130603B modelled in the same manner, and from simulated short GRBs in Ziaeepour & Gardner (2011) with typical fluence and peak energy, as e.g. one can conclude from Fig. 1.

The lower shell density with respect to other short GRBs is necessary to reproduce smaller fluence and peak energy of GRB 170817. In this case, transferring a large fraction of kinetic energy of baryons to electrons seems even more difficult than when shells are denser. Due to smaller cross-section for scattering of particles in a diluted fluid, colliding shells are expected to produce less turbulence and weaker induced electromagnetic field in the shock front. Moreover, low electron yield of neutron rich BNS ejecta should make the transfer of kinetic energy to electrons even harder. Estimation of electron yield Y_e for various components of the ejecta of GW 170817 event based on the observation of r-process products (Hotokezaka et al. 2013; Siegel & Metzger 2017) are $Y_e \sim 0.1-0.4$ for dynamical component, $Y_e \sim 0.3$ for wind, and $Y_e \sim 0.25$ in another wind component (Pian et al. 2017). Considering these yields, and the value of $\epsilon_e Y_e$ in low Lorentz factor simulation No. 2, the effective fraction of kinetic energy transferred to electrons ϵ_e had to be $\sim 0.1-0.3$ to generate a prompt gamma-ray emission with characteristics of GRB 170817A. However, PIC simulations predict that in relativistic shocks $\epsilon_e \lesssim 0.1$ (Spitkovsky 2008; Sironi & Spitkovsky 2011a,b). Therefore, the value of ϵ_e in simulations with low Lorentz factor are at best marginally consistent with PIC simulations. On the other hand, simulations of BNS merger predict (Rezzolla et al. 2011; Kiuchi et al. 2014; Kawamura et al. 2016) that relativistic jet is formed from low electron yield dynamical poleward ejecta. In this case, the value of ϵ_e in our simulations with $\Gamma \sim 10$ would be implausibly high.

One may criticize the above argument because simulations of relativistic shocks with PIC method are still very far from being realistic and predictions for ϵ_e mentioned above are either concluded from PIC simulations of $e^{\pm}$ plasma (Spitkovsky 2008), or from simulations with smaller mass ratio between opposite charges than in electron-proton plasma (Sironi & Spitkovsky 2011a,b; Murphy et al. 2010). None the less, giving the fact that electromagnetic interaction is independent of mass, one expects that in a baryon dominated shock the transferred energy to charged leptons make up an even smaller fraction of total available energy than in $e^{\pm}$ case, despite the fact that the total energy transferred to electromagnetic fields would be larger for the same relative Lorentz factor of colliding shells. Thus, the value of ϵ_e in short GRB jets may be even less than the finding of PIC simulations.

Based on these arguments we conclude that it is unlikely that a structured jet viewed off-axis in a region with $\Gamma \sim 10$ can explain the observed properties of prompt gamma-ray of GRB 170817A, unless the viewing angle was not too far from on-axis or the jet was not strongly structured and Lorentz factor was ∼100, which is only a few folds less than brighter short bursts, such as GRB 130603B.

It is not possible to compare the above conclusion with e.g. analyses of late afterglows by Mooley et al. (2017) and Troja et al. (2018), because there is no evidence of direct relation between the ejecta responsible for these emissions and the prompt ultra-relativistic jet. For instance, Mooley et al. (2017) assume a reduction of Lorentz factor from 3.5 at early times to 2.5 at the time of their observations at $\sim T + 100$ d, and model the afterglows by a shock with $\epsilon_e = 0.1$ and $\epsilon_B = 0.01$ or $\epsilon_B = 0.003$. However, according our arguments about ϵ_e, the value chosen by Mooley et al. (2017) is at upper limit of expected range. Moreover, the initial Lorentz factor is suitable for slow outflows and too low for the production of the prompt gamma-ray. The values of density, ϵ_e and ϵ_B reported in Troja et al. (2018) are consistent with findings of PIC simulations and simulations of afterglow using phenomenological model of Ziaeepour & Gardner (2011), which will be reported elsewhere. But they do not provide any information about the state of ejecta/jet responsible for the prompt gamma-ray. Notably, they do not provide any value for the Lorentz factor at any epoch to compare with our findings.

5.3 Ultra-relativistic jet

Finally, after disfavouring other models, we conclude that the most physically plausible origin of GRB 170817A is synchrotron/self-Compton emission from internal shocks in an ultra-relativistic jet,

which according to the phenomenological model of Ziaeepour (2009) and Ziaeepour & Gardner (2011) its bulk Lorentz factor was ∼100 and densities of colliding shells as reported in simulation No. 1 in Table 2. These values are, respectively, few folds and more than one order of magnitude less than what is expected for typical short GRBs according to the same model. We notice that Murguia-Berthier et al. (2017) have also arrived to a similar conclusion by analysing afterglows of GW/GRB 170817. According to simulation No. 1 in Table 2) such a jet needs $\epsilon_e Y_e \sim 0.01$. Considering estimated values for Y_e of various ejecta of GW 170817 event, we obtain $\epsilon_e \sim 0.03-0.1$, which is comfortably in the range of values observed in PIC simulations. As mentioned in Section 5.2, we cannot rule out that a somehow off-axis view of a mildly structured jet was responsible for reduced Lorentz factor and densities. However, based on arguments given in Section 3, it is more plausible that intrinsic properties of progenitor neutron stars and dynamics of their merger were responsible for the faintness of GRB 170817A. The lack of bright short GRBs at low redshifts is also an additional evidence for this conclusion, see Fig. 1(c,d) and fig. 28 in Lien et al. (2016), which shows the distribution of average flux of *Swift*-BAT GRBs with known redshift(both short and long) and the absence of intrinsically bright bursts at low redshifts.

In the next section we use results from observation of neutron stars, GRMHD simulations of BNS merger, and simulations of jet acceleration to assess what might have been different in GW 170817 event with respect to progenitor of other short GRBs.

6 IMPLICATION FOR PROPERTIES OF GW 170817 PROGENITOR

Which properties of the progenitor neutron stars of GW 170817 event and their merger may have been responsible for lower than usual Lorentz factor of relativistic jet and its lower density, as concluded from our modelling of GRB 170817A ? To answer this question we need a full theoretical and numerical formulation of neutron star physics and NS–NS merger, including: equation of state and interactions of neutron rich material under strong gravity force; magnetic field of progenitor BNS and its evolution during merging event; dynamics of merging, specially its latest stages before formation of a Hyper Massive Neutron Star (HMNS) or a black hole; evolution of accretion disc; evolution of pressurized neutron rich ejecta and its interactions with radiation and neutrino fields; and processes involved in acceleration of particles in the ejecta to ultra-relativistic velocities and formation of a relativistic jet.

Such task highly exceeds our analytical and numerical calculation capabilities. In addition, NS–NS and NS—BH mergers occur at distances of the order of few tens of kilometres, whereas particle acceleration occurs in a magnetically loaded outflow along a distance of at least few orders of magnitude longer (Tchekhovskoy et al. 2008; Komissarov et al. 2009). These two scales cannot be numerically treated with same precision in a same code. Therefore, for relating the results of our modelling of high energy electromagnetic emission and other observations of GW/GRB 170817A to properties of its progenitor, we have to rely on partial and far from ideal models and simulations, which only allow a qualitative assessment of progenitor's characteristics. For this purpose we use mostly, but not exclusively, the results of simulations reported in Kawamura et al. (2016) for NS–NS merger and those of Komissarov et al. (2009) for jet acceleration.

6.1 Equation of state (EoS)

It is by far the most important characteristic of neutron stars and defines the relation between their mass and radius. It also determines other properties such as core and crust densities, tidal deformability, which affects ejecta mass, density, and buoyancy during merger, differential rotation, maximum mass, magnetic field, and formation of an HMNS and its lifetime (Özel & Freire 2016). LIGO–Virgo analysis of GW 170817 event disfavours stiff equations of state (LIGO Scientific Collaboration & Virgo Scientific Collaboration 2017a). Simulations of NS–NS merger in Kawamura et al. (2016) are performed for two equations of state: IF-q[6] consisting of a single polytropic fluid with polytropic index $\Gamma_p = 2$ and polytropic constant $K = 100$; and Hyperon-rich H4 model (Glendenning & Moszkowski 1991). According to classification of NS states in Read et al. (2009), IF-q and H4 are prototypes of soft and stiff equations of state, respectively. We use the results of our simulations to assess which of these models is better consistent with GW/GRB 170817A.

In what concerns state dependent properties, which may affect electromagnetic emission from merger, for close mass NS progenitors the density of inner part of the accretion disc and poloidal magnetic field of the merger are lower in IF-q case than H4 (Kawamura et al. 2016). Although currently no systematic study of the impact of the equation of state on the properties of polar outflow is available, it is known that it is closely related to magnetic field, mass, density, extent of accretion disc (Stepanovs & Fendt 2016), and accretion rate (Blandford & Znajek 1977). The smaller value of these quantities in IF-q means that it also generates less outflow. Thus, we conclude that an equation of state similar to IF-q better represents the state of GW/GRB 170817A progenitor. This independent assessment of EoS is consistent with GW observations, which finds that H4 falls just on the 90 per cent exclusion probability curve for both fast and slow rotating progenitor BNS (LIGO Scientific Collaboration & Virgo Scientific Collaboration 2017a).

6.2 Strength of magnetic field

Simulations of Kawamura et al. (2016) show that for equal mass BNS, after the collapse of HMNS to black hole if the initial magnetic fields of progenitors are aligned with each other and anti-aligned with the rotation axis of the BNS (case DD in nomenclature of Kawamura et al. 2016), the average poloidal magnetic field is about five times weaker than if both initial fields are aligned with rotation axis (case UU). If the initial fields are anti-aligned with each other (case UD), the average poloidal field is even smaller by a few folds. Moreover, in DD and UD cases, the average field at $|\theta| \lesssim 20^\circ$, where θ is the angle between magnetic axis and rotation axis of the merger, is a few times weaker than UU case. A reduced magnetic field proportionally reduces attainable Lorentz factor for material ejected close to polar direction (Komissarov et al. 2009).

If the progenitor neutron stars of GW/GRB 170817A had dipole magnetic fields which extended out of their surface, they should have been surrounded by strongly magnetized atmospheres before their merger. In this case, the magnetic interaction during close encounter of the stars might have disaligned their fields well before the last stages of inspiral, and at the time of merging they were in a state close to UD in the simulations of Kawamura et al. (2016). Moreover, considering the old population of the host galaxy NGC 4993, which have an estimated minimum age of $\gtrsim$1 Gyr (Belczynski et al. 2017;

[6]Nomenclature used in Kawamura et al. (2016).

Blanchard et al. 2017; Im et al. 2017), magnetic fields of progenitors could have been as low as 10^8-10^9G and fast precessing, if the progenitors were recycled millisecond pulsars. The field could be even smaller if they had evolved in isolation (Harding & Lai 2006; Krastev & Li 2010). Such initial field strength is much smaller than $|B| \sim 10^{12}-10^{15}$G used in simulations of BNS merger. Therefore, the magnetic field of the short lived HMNS and accretion disc of the final black hole of GW 170817 also could have been a few orders of magnitude less than $|B| \sim 10^{15}-10^{16}$ G seen in the simulations (Rezzolla et al. 2011; Kiuchi et al. 2014; Kawamura et al. 2016; Ruiz et al. 2016).

6.3 Disc/torus, jet, and accretion rate

Density and initial Lorentz factor of magnetically collimated polar outflow is expected to depend on the Poynting energy carried by the flow. As discussed above, simulations performed with high initial magnetic field of $\sim 10^{15}$ G and equal mass progenitors (Kiuchi et al. 2014) generate a large magnetic field of $\sim 10^{16}$ G for the merger and a relatively large initial Lorentz factor of $\Gamma_i \sim 4$ for the outflow. Simulations with smaller initial magnetic field of $\sim 10^{12}$ G attain a magnetic field of $\sim 10^{13}$G on the disc and a polar outflow with an axial velocity of $\sim 0.3c$, where c is the speed of light (Kawamura et al. 2016). Thus, we expect that if the initial masses of progenitors of GW 170817 were close to each other and their initial magnetic fields similar to those of millisecond pulsars, the magnetic field of the merger could be $\lesssim 10^{10}$ G, which is few orders of magnitude less than what is expected for younger progenitors. Although the velocity of blue ejecta in GW 179817 event is estimated to have been $\sim 0.3c$ (Nicholl et al. 2017; Pian et al. 2017; Smartt et al. 2017), which is similar to what is obtained in simulations with a merger magnetic field of $\sim 10^{13}$G, a larger disc mass and/or density might have partially energized the outflow. The observed low initial velocity of polar outflow and possibility a low magnetic field imply reduced acceleration of particles at high altitudes, and thereby a thin relativistic jet with low Lorentz factor, which could generate a soft and faint GRB consistent with observations and our estimations for characteristics of the ultra-relativistic jet.

In addition to Lorentz factor, the fluence of a GRB depends on the jet extend, i.e. the total amount of ejected and accelerated material. According to simulations of Kawamura et al. (2016) equal mass NS–NS mergers generate less massive and more diluted discs – by a factor of ~ 100 in their inner part – than mergers with a mass ratio of ~ 0.8. In GW/GRB 170817A event progenitor masses were not equal but were close to each other: $M_1 \sim 1.36$–$1.60\,\mathrm{M}_\odot$ and $M_2 \sim 1.17$–$1.36\,\mathrm{M}_\odot$, leading to $M_2/M_1 = 0.855 \pm 0.095$. The upper limit of this mass ratio is close to 1. Thus, the merger might have ejected much less material than NS binaries with larger mass difference or NS–BH mergers, which based on observations of BH–BH merger, are expected to have much larger mass difference. Moreover, relativistic MHD simulations of magnetized jet in Komissarov et al. (2009) show that the reduction of initial total kinetic and Poynting energy by a factor of 2 reduces the density of outflow with highest Lorentz factor by a factor of 5 or so. Both of these observations are consistent with reduced shell densities and extend, and reduced Lorentz factor found in our simulations of GRB 170817A.

Simulations reported in Dionysopoulou et al. (2015) and Kawamura et al. (2016) show that a poloidal coherent magnetic field and an outflow funnel begin to form after the collapse of HMNS to a black hole and outflow rate is correlated with accretion rate from disc/torus (Blandford & Znajek 1977; Stepanovs & Fendt 2016). Giving the fact that the outflow had to be accelerated gradually at high latitudes, a delay between the end of GW and generation of a relativistic jet is expected. It had to be inversely proportional to the strength of poloidal magnetic field and the injection velocity. To this acceleration delay one has to add the time delay between ejection of density shells and their collision (Ziaeepour & Gardner 2011). Furthermore, if the accretion disc was low density and diluted, the accretion rate, and thereby the growth of anisotropies in the ejecta might have been slower than in cases with higher magnetic field and faster accretion. These delays explain the observed delay between the end of GW 170817 maximum and trigger time of GRB 170817A. The origin of the delay is also consistent with arguments we raised to explain low jet density and relatively long duration of GRB 170817A.

6.4 Effect of initial spin

Initial spins of progenitor neutron stars have a crucial role in the dynamics of merging process, in particular in the amount of ejecta, density and extent of accretion disc/torus, and spin of HMNS and black hole. Moreover, they provide information about formation and history of the BNS. GWs from a merger contain information about spins of progenitors and their alignment with orbital rotation axis, see e.g. simulations in Bernuzzi et al. (2014), Dietrich et al. (2017), and Maione et al. (2010). However, in the case of GW 170817 the weakness of the signal and a glitch in LIGO–Livingston data prevented quantitative estimation of progenitors spins.

Binding energy of NS–NS merger is stronger(weaker) for anti-aligned(aligned) initial spins with respect to orbital axis, and leads to shorter(longer) inspiral regime and smaller(larger) ejecta, but significantly depends on the mass ratio of progenitors and is smaller in equal mergers (Bernuzzi et al. 2014). Thus, the direction of differences are similar to those of magnetic field discussed in Section 6.2. However, spin effect on the amount of ejected material is subdominant with respect to other processes and amounts to only few percents (Bernuzzi et al. 2014). On the other hand, the spin of BNS affects the precision of mass determination from GW observations (Brown et al. 2012; LIGO Scientific Collaboration & Virgo Scientific Collaboration 2017b). In the case of GW 170817, variation of normalized angular momentum $a \equiv J/GM^2$, where J is the angular momentum, in the range $0.05 < a < 0.89$ results to mass ranges $M_1 \sim 1.36$–$2.26\,\mathrm{M}_\odot$ and $M_2 \sim 0.86$–$1.36\,\mathrm{M}_\odot$ for NS progenitors (LIGO Scientific Collaboration & Virgo Scientific Collaboration 2017b). However, an error of $\lesssim 50$ per cent on the masses of progenitors and thereby the ejecta alone cannot explain orders of magnitude faintness of GRB 170817A, unless the equation of state changes drastically with mass. Therefore, despite small effect of spins on outflow and jet, their anti-alignment with orbital directions is better consistent with the weak jet of GRB 170817A.

In conclusion, the observed properties of GW and electromagnetic emissions of GW 170817 event are consistent with each others and with our estimation of jet properties in Sections 4 and 5.

7 IMPLICATION OF PROGENITORS PROPERTIES FOR AFTERGLOW OF GW/GRB 170817 AND OTHER SHORT GRBS

Formation of a GRB is the manifestation of just one component of complicated events which occur during merger of BNSs. Therefore, any argument for unusual properties of GRB 170817A must be also consistent with low energy afterglows and emissions from other components of the merger remnant. Here, we verify whether properties of the progenitor neutron stars and their merger discussed

in the previous section, which may explain the faintness of GRB 170817A prompt gamma-ray, are compatible with low energy observations.

7.1 Evidence from UV/optical/IR/radio counterparts

From UV/optical/IR/radio observations various conclusions are made in the literature about properties of the progenitors and their merger, which are not always consistent with each other and with numerical simulations. Here is a summary of conclusions and some of inconsistencies:

(i) The merger made an HMNS which after ∼10 ms or so collapsed to black hole. This is a common conclusion in the literature (Kasen et al. 2017; Pian et al. 2017). The strongest evidence is the fact that much larger ejecta – presumably from accretion disc around a black hole – is necessary for explaining observed luminosity of the optical counterpart AT 2017 gfo than tidally stripped tail of the merger can provide (Maione et al. 2010; Tanaka & Hotokezaka 2013; Bernuzzi et al. 2014; Sekiguchi et al. 2016; Dietrich et al. 2017; Tanaka et al. 2018).

(ii) According to predictions of theoretical models, AT 2017 gfo was a red kilonova, meaning that heavy r-processes occurred in a dense optically thick material ejected from an accretion disc/torus (Kasen et al. 2017).

(iii) The early bright blue/UV emission (Evans et al. 2017) observed at $\lesssim T + 1.5$ d is from a Lanthanide-free low density post-merger squeezed polar wind consisting of light elements and having a relatively large electron yield of $Y_e \sim 0.25-0.3$ (Hotokezaka et al. 2013; Kasen et al. 2017; Pian et al. 2017; Tanaka et al. 2018). Observation of this component may imply that the viewing angle of observer must have been close to polar to be able to detect it. As in NS–NS merger the toroidal field is always much stronger than poloidal one (Kawamura et al. 2016), polarization of photons should be mainly parallel to the jet axis. The absence of linear polarization even at early times (Covino et al. 2017) is an evidence for scattering of photons in a turbulent funnel rather than direct sideway view of the ejecta on the surface of sky.

(iv) There is not a general consensus about the amount of ejected mass and contribution of different components: dynamical tidal tail; poleward outflow, cocoon, and wind; and post-merger close to spherical ejecta due to the heating of the accretion disc/torus. Observations can only rule out a one-component thermally evolving ejecta (Arcav et al. 2017; Pian et al. 2017).

(v) Velocity of ejecta defined as $v_{ej} \equiv E/2M_{ej}$ is estimated to be $v_{ej} \sim 0.2 - 0.3c$ at $\sim T + 1.5$ d. Simulations predicts such a velocity for poleward dynamical tail material at ejection (Rezzolla et al. 2011; Dionysopoulou et al. 2015; Kawamura et al. 2016; Ruiz et al. 2016).

(vi) Based on analysis of optical/IR/radio observations of AT 2017 gfo the ejecta mass responsible for the observed r-process rich spectrum is estimated to be as high as $M_{ej} \sim 0.03-0.05\,M_\odot$ and its velocity as mentioned above (Arcav et al. 2017; Pian et al. 2017; Smartt et al. 2017). However, this is much larger than $\sim 0.01\,M_\odot$ predicted by simulations for the fast outflow. It is also ∼3−5times larger than tidal ejecta mass estimated for the bright short GRB 130603B, which was accompanied by a kilonova event (Berger et al. 2013; Tanvir et al. 2013).

(vii) At about $T + 100$ d X-ray, optical and radio afterglow do not show any signature of a relativistic jet (Mooley et al. 2017; Margutti et al. 2018; Lazzati et al. 2017b). These observations are consistent with a slow evolving ejecta component and with a weak ultra-relativistic jet, which at this late times should be most probably dissipated by interacting with circumburst material.

The tidally stripped dynamical ejecta is expected to be cold and to have high Y_e and light-element composition due to interaction with released neutrinos (Maione et al. 2010). These predictions are consistent with observations. However, GRMHD simulations of BNS merger estimate a mass of $10^{-3}-10^{-2}\,M_\odot$ for dynamical ejecta, irrespective of progenitors mass ratio and equations of state (Maione et al. 2010; Bernuzzi et al. 2014; Dietrich et al. 2017; Kasen et al. 2017). Therefore, a contribution from post-merger ejected material from an accretion disc/torus seems necessary to explain the data. Moreover, this additional early ejecta should become optically thin and observable in UV and visible bands as early as $\sim T + 0.6$ d (Arcav et al. 2017; Pian et al. 2017). However, simulations also predict that post-merger wind would have a low velocity of $0.02-0.1c$ and high opacity (Maione et al. 2010; Hotokezaka et al. 2013; Sekiguchi et al. 2016; Dietrich et al. 2017; Tanaka et al. 2018).

It is shown (Pian et al. 2017) that the optical/IR spectrum during $T + 0.6$ d to $T + 1.5$ d can be reproduced by a three-component model constructed according to simulations of Sekiguchi et al. 2016) and Tanaka et al. (2018): a $Y_e = 0.1-0.4$ component representing dynamical tidal tail ejecta with a velocity of $\sim 0.2c$; and two components with $Y_e = 0.25$ and $Y_e = 0.3$ and a low velocity of $\sim 0.05c$ representing post-merger ejecta. A scaling of the simulated spectra, which was performed for $M_{ej} = 0.01\,M_\odot$, is necessary to obtain a correct amplitude for the spectrum of At 2017 gfo. However, thermal evolution of this model does not reproduce later spectra (Pian et al. 2017). Moreover, even in the earliest time interval, the contribution of slow components – presumably from disc – is subdominant and does not solve the problem of too large ejecta mass mentioned above. Therefore, despite overall agreement, current predictions of BNS merger simulations poorly fit the AT 2017 gfo data (Arcav et al. 2017; Buckley et al. 2017; Coulter et al. 2017; Pian et al. 2017; Smartt et al. 2017; Valenti et al. 2017).

We should also remind that in Kawamura et al. (2016) a velocity of $\sim 0.3c$ for post-merger magnetically loaded polar outflow is reported only for H4 equation of state. For a softer state the velocity is expected to be less. In addition, as we discussed earlier, a weaker magnetic field reduces both the amount and velocity of the outflow at ejection time (Stepanovs & Fendt 2016). And although the ejecta continues to be somehow collimated, it should have a larger opening angle. Because the polar wind is accelerated by dissipation of Poynting energy after its ejection (Komissarov et al. 2009), the effect of low ejection velocity may be smeared out by acceleration at high latitudes. At present simulations of BNS merger does not include these late processes. Moreover, acceleration of charged particles segregates them from neutron-rich component and increase the effective Y_{ej} in the fast outflow. Energy dissipation of neutrinos may also be involved in increasing the velocity of initially slow ejecta from accretion disc (Martin et al. 2015). However, most GRMHD simulations do not include a full treatment of neutrinos and their predictions may be unrealistic.

Another solution for resolving inconsistencies, as we discussed in Section 2.1 and also suggested in Arcav et al. (2017), is a contribution from the afterglow of GRB 170817A in the observed blue peak during $T + 0.6$ d to $T + 1.5$ d. In this case, less early ejecta would be necessary to explain observations. Indeed, analysis of bolometric light curve in Smartt et al. (2017) shows that if the bluest data points of the spectrum at $\sim T + 0, 6 - T + 1.5$ d are not included in the fit and a thermalization efficiency is added to the model, a smaller ejecta mass of $\sim 0.018\,M_\odot$ and a larger opacity – a sig-

nature of higher atomic mass elements, presumably from accretion disc – fit the data better. Thus, the blue part of the early optical spectrum needs another component of the ejecta. This analysis is another evidence that the early non-thermal blue emission was at least partially due to the afterglow of the relativistic jet, which at times $\gtrsim T + 0.5$ d was significantly slowed-down by shocks and internal dissipation. Even at $\sim T + 110$ d observation of optical counterpart shows that it is too bright and blue to be consistent with kilonova emission alone and a contribution from GRB 170817A afterglow seems necessary to explain observations (Lyman et al. 2018). Unfortunately, in absence of an early observation of optical and X-ray afterglow, it is not possible to estimate the contribution of synchrotron emission from the GRB afterglow in the observed blue peak.

Late observations of optical/IR (Lyman et al. 2018) and X-ray (Lazzati et al. 2017b; Margutti et al. 2018) observations of GW 170817 counterparts are found to be consistent with off-axis structured jet (Lazzati et al. 2017b) and with both the latter model and cocoon models (Margutti et al. 2018). Moreover, with the assumption of an off-axis viewing angle and structured jet, a broad-band analysis of late afterglows rules out top hat (uniform) and power-law jet profiles and simplest cocoon model (Troja et al. 2018), but finds that a Gaussian jet profile or a cocoon with energy injection are consistent with data. However, the models studied in Margutti et al. (2018) are only at 2σ level consistent with the early epoch Chandra data. Additionally, radio observations at roughly the same epoch of X-ray and optical/IR observations are not consistent with off-axis view of a structured jet and need a quasi-spherical mildly relativistic outflow (Mooley et al. 2017). It may be an evidence for a cocoon around a relativistic jet, as predicted by simulations. Alternatively, the brightening of radio and higher energy emissions can be due to high velocity tail of neutron rich dynamical ejecta (Hotokezaka et al. 2018). For instance, continuous heating and evaporation of the outer part of the accretion disc and reduction of opacity its due to expansion may explain gradual brightening and the need for energy injection found by (Troja et al. 2018). Collision of outflow with the ISM is another possibility. All these models predict the decline of emission, which seems to have begun at $\lesssim T + 134$ d (D'Avanzo et al. 2018). Although there is not yet enough data to allow discrimination between models studied in Mooley et al. (2017), Troja et al. (2018), and D'Avanzo et al. (2018), some of off-axis models, such as those simulated in Lazzati et al. (2017b) with a viewing angle $\theta \gtrsim 16^\circ$ are ruled out. Moreover, models which best-fitting late observations in X-ray and radio according to Lazzati et al. (2017b, see their figs. 2, 3, and 4) are ruled out, because they predict the brightening of afterglow for at least few hundreds of days, which is inconsistent with the decline observed in X-ray and optical by D'Avanzo et al. (2018).

In any case, as we argued in Section 5.2, the ejecta component(s) responsible for the late afterglow may have little direct relation with the relativistic jet that generated prompt gamma-ray, except probably some contribution from external shock of the relativistic jet. However, external shocks depend on surrounding material and do not directly present the state of ultra-relativistic jet to be compared with our conclusions.

7.2 A qualitative picture of GW/GRB/kilonova 170817

Finally, our interpretation of data and simulations of GW/GRB/kilonova 170817 can be summarized in the following qualitative picture:

(i) Progenitors were old and cool neutron stars with close masses, i.e. $M_2/M_1 \lesssim 1$.

(ii) They had soft equations of state and small initial magnetic fields of $\lesssim 10^9$ G. Their fields were anti-aligned with respect to orbital rotation axis and each other.

(iii) For dynamical or historical reasons, such as encounter with similar mass objects, their spins before final inspiral were anti-aligned.

(iv) The merger produced an HMNS with a moderate magnetic field of $\lesssim 10^{10}$ G. This value is in the lowest limit of what is obtained in GRMHD simulations.

(v) The HMNS eventually collapsed to a black hole and created a moderately magnetized disc/torus and a low density, low magnetized, and mildly collimated polar outflow.

(vi) A total amount of $\sim 0.03-0.05\,\mathrm{M}_\odot$ material, including $10^{-3}-10^{-2}\,\mathrm{M}_\odot$ of tidally stripped pre-merger and a post-merger wind were ejected to high latitudes. They were subsequently collimated and accelerated by transfer of Poynting to kinetic energy. The same process increased electron yield by segregation of charged particles.

(vii) A small mass fraction of the polar ejecta was accelerated to ultra-relativistic velocities and made a weak GRB. The reason for low Lorentz factor, density, and extent of this component was the weakness of the magnetic field.

(viii) Either due to the weakness of the relativistic jet, which soon after internal shocks had a break and lost its collimation, or due to the lack of sufficient circumburst material, the afterglows of the GRB in X-ray and lower energy bands were very faint at $\gtrsim T + 0.6$ d, and only detectable as a non-thermal addition in UV/blue emission of cocoon/wind.

(ix) The late X-ray brightening is most probably independent of unusual weakness of GRB 170817A and is generated by interaction of a slower component of ejecta with the ISM or other surrounding material. The remnant of the relativistic jet may have some contribution in these emissions, specially at earlier times.

At present faint GRBs similar to GRB 170817A are detectable by high energy satellites only if they occur in the local Universe. Therefore, the small accessible volume significantly suppresses the rate of such events. Indeed, since the launch of the *Swift* satellite until present only 7 confirmed short bursts without early X-ray counterpart[7] were observed.[8] In addition, association of these transients to BNS merger is not certain and some of them may be giant flares from SGRs in nearby galaxies. Only long duration follow-up of future early time X-ray faint or dark GRBs with or without associated GW can prove or refute hypotheses raised here to explain the unusual characteristics of GRB 170817A.

7.3 Progenitors of bright short GRBs

Due to observational bias most of GRBs with known redshift or their host galaxies are bright. If our explanation of reasons behind the weakness of GRB 170817A are correct, BNS mergers at higher redshifts must be on average intrinsically brighter, because

[7]By early afterglow we mean from $\gtrsim T+$ 100 s up to $\sim T + \mathcal{O}(1) \times 10^4$ s. Usually if no X-ray afterglow is found in this interval, no further detection attempt would be made. GRB 170817A was an exception due to its association with a GW event.

[8]According to our search in the on-line *Swift*-BAT data base https://swift.gsfc.nasa.gov/archive/grb_table/.

younger neutron stars have stronger magnetic fields. Their spin–orbit orientation is a priori independent of redshift, but it should somehow depend on age, formation history, and environment of the BNS. Older binaries on average had more opportunity to interact with other celestial bodies. For instance, neutron stars in the dense environment of globular clusters have higher chance of forming BNS and being gravitationally disrupted, which may change their spin–orbit orientation.

Despite small number of short GRBs with known redshift, the impact of BNS aging on the outcome of the merger gradually become discernible in the data. Indeed, in Fig. 1(c,d) there is a clear trend of increasing total fluence and average flux with redshift. Although the absence of faint bursts at higher redshifts can be interpreted as an observational bias, the lack of bright bursts at lower redshifts is not explainable and their rarity does not seem sufficient to explain clear stratification of fluence and average flux with redshift.

Although no BH–NS merger is so far detected, they remain a plausible origin for energetic short GRBs, because the larger mass difference of the pair may produce larger ejecta and magnetic field (Kawaguchi et al. 2015; Kiuchi et al. 2015; Paschalidis, Ruiz & Shapiro 2015; Foucart et al. 2016). Only with detection of more GW events with electromagnetic counterparts it would be possible to verify this hypothesis.

8 OUTLINE

GW/GRB 170817A event gave us the opportunity to discover the nature of short GRBs, which for decades their origin was a subject of speculation and no direct evidence or proof of hypotheses about their sources was in hand.

In this work through simulation of prompt emission of GRB 170817A we showed that despite its outlier characteristics, it was generated by the same physical processes involved in the production of more ordinary and typical short GRBs. Based on the results of 3D GRMHD from the literature and published analysis of multi-wavelength observations of this event we argued that the faintness of GRB 170817A was caused by old age, coolness, and reduced magnetization of its progenitor neutron stars. These intrinsic factors were probably helped by environmental effects and history of gravitational disturbances, which had induced an anti-aligned spin–orbit orientation.

Current observation facilities, specially GW detectors, are sensitive to events similar to GW/GRB 170817 only if they occur at redshifts $\lesssim$0.1. Moreover, despite the ability of the *Swift* satellite to detect the counterpart of GRBs in X-ray, UV, and white bands from on average $\gtrsim$70 s onward, since its launch in November 2004 only a very small fraction of short GRBs have had long duration follow up, i.e. for more than few days, either by the *Swift* instruments, or by other ground- and space-based telescopes. For this reason, the state of our knowledge about late behaviour of their afterglow and associated physical processes is incomplete. None the less, there is hope that the huge scientific outcome achieved from intense observation of GW/GRB 170817A/AT 2017 gfo, which was a first in its kind, would encourage more intense and long duration follow up of short GRBs, even without any associated GW. Such observations would help verify some of hypotheses suggested in this work about the progenitors of short GRB/kilonova events. For instance, whether the late brightening of their afterglow is a common behaviour, and whether there is any systematic correlation between age and star formation history of their host galaxies and properties of NS–NS and NS–BH mergers.

ACKNOWLEDGEMENTS

The author thanks Phil Evans for providing her with *Swift*-XRT data before their publication.

REFERENCES

Alexander K. D. et al., 2017, ApJ, 848, L21
Aptekar R. L. et al., 1995, Space Sci. Rev., 71, 265
Arcavi I. et al., 2017, Nature, 551, 64
Asano K., Inoue S., Meszaros P., 2010, ApJ, 725, 121
Belczynski K. et al., 2017, preprint (arXiv:1712.00632)
Berger E., 2014, ARA&A, 52, 43
Berger E., Cenko S. B., Fox D. B., Cucchiara A., 2009, ApJ, 704, 877
Berger E., Fong W., Chornock R., 2013, ApJ, 774, L23
Bernuzzi S., Dietrich T., Tichy W., Bruegmann B., 2014, Phys. Rev. D, 89, 104021
Blackman E. G., Yi I., Field G. B., 1996, ApJ, 473, L79
Blanchard P. K. et al., 2017, ApJ, 848, L22
Blandford R. D., Znajek R. L., 1977, MNRAS, 179, 433
Bromberg O., Tchekhovskoy A., 2016, MNRAS, 456, 1739
Brown D. A., Harry I., Lundgren A., Nitz A. H., 2012, Phys. Rev. D, 86, 084017
Buckley D. A. H. et al., 2018, MNRAS, 474, L71
Burgess J. M. et al., 2014, ApJ, 784, 17
Chornock R. et al., 2017, ApJ, 848, 19
Coulter D. A. et al., 2017, Science, 358, 1556
Covino S. et al., 2017, Nat. Astron., 1, 791
Cowperthwaite P. S. et al., 2017, ApJ, 848, 17
Cuesta-Martínez C., Aloy M. A., Mimica P., 2015a, MNRAS, 446, 1716
Cuesta-Martínez C., Aloy M. A., Mimica P., Thöne C., de Ugarte Postigo A., 2015b, MNRAS, 446, 1737
Cummings J. R. et al., 2006, GCN Circ., 5301
D'Avanzo P. et al., 2018, A&A, 613, L1
D'Elia V., Chester M. M., Cummings J. R., Malesani D., Markwardt C. B., Page K. L., Palmer D. M., 2013, GCN Circ., 15212
De Colle F., Lu W., Kumar P., Ramirez-Ruiz E., Smoot G., 2018, MNRAS, doi:10.1093/mnras/sty1282
De Pasquale M. et al., 2006, GCN Circ., 5409
Dietrich T., Bernuzzi S., Ujevic M., Tichy W., 2017, Phys. Rev. D, 95, 044045
Dingus B. L., 1995, Space Sci., 231, 187
Dionysopoulou K., Alic D., Rezzolla L., 2015, Phys. Rev. D, 92, 084064
Evans P. A., Osborne J. P., Willingale R., O'Brien P. T., 2011 , in McEnery I. E., Racusin J. L., Gehrels N., eds., AIP Conf. Proc. Vol. 1358, Gamma Ray Bursts 2010 , Am. Inst. Phys., New York, p. 117.
Evans P. A. et al., 2017, Science, 358, 1565
Fargion D., 2003, Chin. J. Astron. Astrophys., 3, 472
Fishman G. J. et al., 1999, in Johnson W. N., ed., Proc. GRO Science Workshop . NASA/GSFC, Greebelt, p. 2
Fong W. F. et al., 2013, ApJ, 780, 118
Foucart F. et al., 2017, Class. Quantum Gravity, 34, 044002
Frederiks D. Konus-Wind Collaboration, 2013, GCN Circ., 14772
Gehrels N. et al., 2004, ApJ, 611, 1005
Ghisellini G. et al., 2012, Proc. Sci., Gamma-Ray Bursts 2012 Conference (GRB 2012). SISSA, Trieste, PoS#015
Glendenning N. K., Moszkowski S. A., 1991, Phys. Rev. Lett., 67, 2414
Goldstein A., Veres P., Burns E., Briggs M. S., Hamburg R., Kocevski D., Wilson-Hodge C. A., Preece R. D., 2017, ApJ, 848, L14
Golenetskii S. et al., 2013, GCN Circ., 14771
Gottlieb O., Nakar E., Piran T., Hotokezaka K., 2018, MNRAS, doi:10.1093/mnras/sty1462
Grubbs F. E., 1969, Technometrics, 11, 1
Gruber D. et al., 2014, ApJS, 211, 27
Guidorzi C. et al., 2017, ApJL, 851, L36
Haggard D., Nynka M., Ruan J. J., Kalogera V., Cenko S. B., Evans P. A., Kennea J. A., 2017, ApJ, 848, L25
Hallinan G. et al., 2017, Science, 358, 1579

Harding A. K., Lai D., 2006, Rep. Prog. Phys., 69, 2631
Hotokezaka K., Kyutoku K., Okawa H., Shibata M., Kiuchi K., 2011, Phys. Rev. D, 83, 124008
Hotokezaka K., Kiuchi K., Kyutoku K., Okawa H., Sekiguchi Y. I., Shibata M., Taniguchi K., 2013, Phys. Rev. D, 87, 024001
Hotokezaka K., Kiuchi K., Shibata M., Nakar E., Piran T., 2018, preprint (arXiv:1803.00599)
Im M. et al., 2017, ApJ, 849, L16
Ioka K., Murase K., Toma K., Nagataki S., Nakamura T., 2007, ApJ, 670, L77
Kasen D., Metzger B., Barnes J., Quataert E., Ramirez-Ruiz E., 2017, Nature, 551, 80
Kasliwal M. M. et al., 2017a, Science, 358, 1559
Kasliwal M. M., Korobkin O., Lau R. M., Wollaeger R., Fryer C. L., 2017b, ApJ, 843, L34
Kathirgamaraju A., Barniol Duran R., Giannios D., 2018, MNRAS, 473, L121
Kawaguchi K., Kyutoku K., Nakano H., Okawa H., Shibata M., Taniguchi K., 2015, Phys. Rev. D, 92, 024014
Kawamura T., Giacomazzo B., Kastaun W., Ciolfi R., Endrizzi A., Baiotti L., Perna R., 2016, Phys. Rev. D, 94, 064012
Kennea J. A. et al., 2013, GCN Circ., 14749
Kiuchi K., Kyutoku K., Sekiguchi Y., Shibata M., Wada T., 2014, Phys. Rev. D, 90, 041502
Kiuchi K., Sekiguchi Y., Kyutoku K., Shibata M., Taniguchi K., Wada T., 2015, Phys. Rev. D, 92, 064034
Kocevski D., Thone C. C., Ramirez-Ruiz E., Bloom J. S., Granot J., Butler N. R., Perley D. A., Modjaz M., 2010, MNRAS, 404, 963
Komissarov S., Vlahakis N., Konigl A., Barkov M., 2009, MNRAS, 394, 1182
Krastev P. G., Li B. A., 2010, APS, CAL, C3001
Lamb G. P., Kobayashi S., 2017, MNRAS, 472, 4953
Lazzati D., Deich A., Morsony B. J., Workman J. C., 2017a, MNRAS, 471, 1652
Lazzati D., Perna R., Morsony B. J., López-Cámara D., Cantiello M., Ciolfi R., Giacomazzo B., Workman J. C., 2017b, preprint (arXiv:1712.03237)
Levinson A., Begelman M. C., 2013, ApJ, 764, 148
Lien A. et al., 2016, ApJ, 829, 47
LIGO Scientific Collaboration, Virgo Scientific Collaboration, 2017a, Phys. Rev. Lett., 119, 161101
LIGO Scientific Collaboration, Virgo Scientific Collaboration, 2017b, ApJ, 850, L40
LIGO Scientific Collaboration, 2017a, ApJ, 848, L12
LIGO Scientific Collaboration, 2017b, ApJ, 848, L13
Link B., 2003 , in Bailes M., Nice D. J., Thorsett S. E., ASP Conf. Ser. Vol. 302, Radio Pulsars. Astron. Soc. Pac., San Francisco, p. 241
Lyman J. D. et al., 2018, preprint (arXiv:1801.02669)
Lyutikov M., Blandford R. D., 2003, preprint (astro-ph/0312347)
Maione F., De Pietri R., Feo A., Löffler F., 2016, Class. Quantum Gravity, 33, 175009
Margutti R. et al., 2017, ApJ, 848, L20
Margutti R. et al., 2018, ApJL, 956, L18
Martin D., Perego A., Arcones A., Thielemann F. K., Korobkin O., Rosswog S., 2015, ApJ, 813, 2
Melandri A. et al., 2013, GCN Circ., 14735
Metzger B. D., 2017, preprint (arXiv:1710.05931)
Mooley K. P. et al., 2018, Nature, 554, 207
Morsink S. M., Stella L., 1999, ApJ, 513, 827
Murase K., Asano K., Terasawa T., Meszaros P., 2012, ApJ, 746, 164
Murase K. et al., 2018, ApJ, 854, 60
Murguia-Berthier A., Ramirez-Ruiz E., Kilpatrick C. D., Foley R. J., Kasen D., Lee W. H., Piro A. L., Coulter D. A., 2017, ApJ, 848, L34
Murphy G. C., Dieckmann M. E., O'C Drury L., 2010, IEEE Trans. Plasma Sci., 38, 2985
Nakar E., Piran T., 2016, ApJ, 834, 28
Nakar E., Sari R., 2012, ApJ, 747, 88
Nicholl M. et al., 2017, ApJ, 848, 18
Oates S. R. et al., 2009, GCN Circ., 10148
Ogilvie G. I., Dubus G., 2001, MNRAS, 320, 485
Paciesas W. S. et al., 2012, ApJS, 199, 19
Paschalidis V., Ruiz M., Shapiro S. L., 2015, ApJ, 806, L14
Pe'er A., Mészáros P., Rees M. J., 2006, ApJ, 642, 995
Pian E. et al., 2017, Nature, 551, 67
Piro L. et al., 2014, ApJ, 790, 15
Pozanenko A. et al., 2018, ApJ, 852, L30
Read J. S., Lackey B. D., Owen B. J., Friedman J. L., 2009, Phys. Rev. D, 79, 124032
Rees M. J., Mészáros P., 2005, ApJ, 628, 847
Rezzolla L., Giacomazzo B., Baiotti L., Granot J., Kouveliotou C., Aloy M. A., 2011, ApJ, 732, L6
Ruiz M., Lang R. N., Paschalidis V., Shapiro S. L., 2016, ApJ, 824, L6
Rybicki G. B., Lightman A. P., 2004, Radiative Processes in Astrophysics. Wiley-VCH verlag GmbH & Co. KGaA , Weinheim
Sakamoto T. et al., 2011, GCN Circ., 12460
Savchenko V. et al., 2017, ApJ, 848, L15
Sekiguchi Y., Kiuchi K., Kyutoku K., Shibata M., Taniguchi K., 2016, Phys. Rev. D, 93, 124046
Siegel D. M., Metzger B. D., 2017, Phys. Rev. Lett., 119, 231102
Siegel M. H., Barthelmy S. D., Burrows D. N., Lien A. Y., Marshall F. E., Palmer D. M., Sbarufatti B., 2016, GCN Circ., 19833
Sironi L., Spitkovsky A., 2011a, ApJ, 726, 75
Sironi L., Spitkovsky A., 2011b, ApJ, 741, 39
Smartt S. J. et al., 2017, Nature, 551, 75
Soares-Santos M. et al., 2017, ApJ, 848, L16
Spitkovsky A., 2008, ApJ, 682, 5
Stepanovs D., Fendt C., 2016, ApJ, 825, 14
Svinkin D. et al., 2017, GCN Circ., 21746
Tanaka M., 2016, Adv. Astron., 2016, 6341974
Tanaka M., Hotokezaka K., 2013, ApJ, 775, 113
Tanaka M. et al., 2018, ApJ, 852, 109
Tanvir N. R., Levan A. J., Fruchter A. S., Hjorth J., Hounsell R. A., Wiersema K., Tunnicliffe R., 2013, Nature, 500, 547
Tchekhovskoy A., McKinney J. C., Narayan R., 2008, MNRAS, 388, 1365
Troja E. et al., 2017, Nature, 551, 71
Troja E., et al., 2018, MNRAS, 478, L18
Tunnicliffe R. L. et al., 2014, MNRAS, 437, 1495
Valenti S. et al., 2017, ApJ, 848, L24
Wijers R., 2018, Nature, 554, 178
Winkler C. et al., 2003, A&A, 411, L1
Zhang B. B., Qin Y. P., 2005, preprint (astro-ph/0504070)
Zhang B., Yan H., 2011, ApJ, 726, 90
Zhao X. H., Li Z., Bai J., 2010, ApJ, 726, 87
Zhu B., Zhang F. W., Zhang S., Jin Z. P., Wei D. M., 2015, A&A, 576, A71
Ziaeepour H., 2009, MNRAS, 397, 361
Ziaeepour H., Gardner B., 2011, J. Cosmol. Astropart. Phys., 12, 001
Ziaeepour H., Barthelmy S. D., Parsons A., Page K. L., De Pasquale M., Schady P., 2007, GCN Rep., 74.2
Özel F., Freire P., 2016, ARA&A, 54, 401

APPENDIX A: EVOLUTION MODELS OF ACTIVE REGION

In the phenomenological model of Ziaeepour (2009), the evolution of $\Delta r'(r')$ cannot be determined from first principles. For this reason we consider the following phenomenological models:

$$\Delta r' = \Delta r'_0 \left(\frac{\gamma'_0 \beta'}{\beta'_0 \gamma'} \right)^{\tau} \Theta(r' - r'_0) \quad \text{dynamical model, Model = 0,} \tag{A1}$$

$$\Delta r' = \Delta r'_\infty \left[1 - \left(\frac{r'}{r'_0} \right)^{-\delta} \right] \Theta(r' - r'_0) \quad \text{Steady state model, Model = 1,} \tag{A2}$$

$$\Delta r' = \Delta r'_0 \left(\frac{r'}{r'_0}\right)^{-\delta} \Theta(r' - r'_0) \quad \text{Power-law model, Model = 2,} \tag{A3}$$

$$\Delta r' = \Delta r_\infty \left[1 - \exp(-\frac{\delta(r' - r'_0)}{r'_0})\right] \Theta(r - r'_0)$$
Exponential model, Model = 3, (A4)

$$\Delta r' = \Delta r'_0 \exp\left(-\delta \frac{r'}{r'_0}\right) \Theta(r' - r'_0)$$
Exponential decay model, Model = 4. (A5)

The initial width $\Delta r'(r'_0)$ in Model = 1 and 3 is zero. Therefore, they are suitable for description of initial formation of an active region in internal or external shocks. Other models are suitable for describing more moderate growth or decline of the active region. In Table 2, the column *mod*. indicates which evolution rule is used in a simulation regime – as defined in the footnotes of this table – using model number given in (A1)–(A5).

This paper has been typeset from a TEX/LATEX file prepared by the author.